Statistical Learning of Passive Infrared (PIR) Sensor Data for Human Monitoring Applications

Submitted by
Jack Andrews

Bioengineering

To
The Honors College
Oakland University

In partial fulfillment of the
requirements to graduate from
The Honors College

Mentor: Dr. Jia Li
Electrical and Computer Engineering Department
Oakland University

April 2, 2021

Table of Contents

Abstract ……...3
Introduction ……4
Background ……8
PIR Sensors ……8
Heart-Related Biometrics ……..10
Performance Metrics ……11
Related Work ……12
PIR Sensors ……...13
Human Monitoring ……....14
Biometrics ……16
Motion Induced PIR Sensor (MI-PIR) ……..18
Data Acquisition ……...19
Office Environment ……..22
Residential Environment ……...24
Data Pre-Processing ……..25
Statistical Learning ……...28
Classifications ……...30
Precise Indoor Localization ……..32
System Quantifications ……34
Visualizations ……38
Chest Motion PIR Sensor (CM-PIR) ……40
Data Acquisition ……...40
Data Pre-Processing ……..42
Deep Learning ……...47
Human Presence ……47
Biometric Authentication ……..48
System Quantifications ……49
Visualizations ……50
Discussion ……53
Conclusions ……...56
Acknowledgements ……...58
References ……58

Abstract

Elderly individuals, especially those who suffer from neurodegenerative diseases, are prone to cognitive impairment and deteriorating motor stability. Moreover, with the emerging field of the internet of things (IoT), security of the data shared throughout these connected devices is a growing challenge, leading to the advancement of the field of biometrics. Passive infrared (PIR) sensors are commonly deployed in related monitoring and security applications as they are cheap, non-contact, commercial-off-the-shelf (COTS) components that have proven to be relatively accurate. PIR sensors function by detecting human presence through a change in infrared radiation across the field of the view (FoV) of the sensor. As a result, the major known drawback with PIR sensors is their inability to reliably detect stationary human occupants. Towards expanding the applications and accuracy of PIR sensors, two methods for detecting stationary human subjects are developed and presented: a motion induced PIR sensor (MI-PIR) and a chest motion PIR sensor (CM-PIR). MI-PIR artificially induces the motion necessary for accurate human detection via a robotic actuator, while CM-PIR relies on the movement of the human chest for accurate detection of stationary subjects. The efficacy of these human presence classifications using a single PIR sensor, as well as related human monitoring classifications and regressions, is dependent on statistical learning algorithms for differentiation of scenarios that exist between the numerous applications. A recurrent neural network (RNN) deep learning model with long short-term memory (LSTM) units is found to be superior for PIR sensor data classification due to the time-series nature of the data, and a Gaussian process regression (GPR) machine learning model is utilized as a regression approach for precise indoor localization. The results of this work show that MI-PIR and CM-PIR are both accurate systems for stationary human presence detection and related human monitoring applications using a single PIR sensor.

Statistical Learning of Passive Infrared (PIR) Sensor Data for Human Monitoring Applications

Introduction

Falls are the leading cause of death in the elderly population [1]. Elderly individuals, especially those that suffer from neurodegenerative diseases such as Alzheimer's disease (AD) and Parkinson's disease (PD), traditionally require monitoring by a caregiver or hospital system to prevent any adverse events or properly respond in case of such an event. The mental and monetary cost of such monitoring places a large burden on both loved ones and the hospital system for basic everyday monitoring of elderly individuals. With 35% of the current medical spending in the United States accounting for the elderly populations 65 years or older, and with this population expected to double in the next thirty years, there exists a need for an at-home monitoring system to alleviate the burden caused by potential harmful activities resulting from the deteriorating motor stability and cognitive ability of elderly individuals [2], [3].

The internet of things (IoT) is a relatively new phenomena that defines the interconnection of devices that are connected to the internet. These devices range from phones, kitchen items, speakers, cars, televisions, and many others [4]. Security of these connected devices is an ever-growing challenge as potential adversaries can gain access to household items and personal data through the forgery of current security systems such as passwords and fingerprinting technology. Fingerprints utilized as a password for security purposes such as in the case of common Apple products relates to the field of biometrics. Biometrics can be defined as the usage of unique biological characteristics for enhanced security such as in the case of fingerprints, facial recognition, and heart-related qualities. Biometric authentication and biometric identification are two classifications that use biometrics for which authentication relates to the classification of one

verified individual against all other adversaries and identification relates to the classification of each individual present in the dataset. Where fingerprints can be easily stolen via the extraction of touched surfaces and where facial recognition solutions are privacy-intrusive and dependent on proper lighting quality, heart-related biometrics are growing in popularity due to both their indication of liveliness and their difficulty of replication. With the number of IoT devices expected to increase, the security of these devices remains a consistent challenge [5].

Ambient sensors and statistical learning algorithms have been applied to develop systems to combat the challenges associated with the current elderly monitoring and IoT security systems presented above. Ambient sensors are more adequate in long-term solutions due to the non-contact nature of detection, which in turn helps eliminate the excessive burden placed on the end-user to carry a terminal device. Ambient sensors such as cameras, thermal sensors, depth sensors, and passive infrared (PIR) sensors, as well as ambient signals such as radio frequency (RF) signals and Wi-Fi channel state information (CSI), all have been leveraged in monitoring systems in related work. Moreover, cameras and Doppler radar scanners have been utilized for IoT security in terms of biometric authentication and biometric identification classifications. Statistical learning algorithms relates to the usage of artificial intelligence (AI) algorithms for learning of the multiple scenarios that exist within a complex dataset such as those existing from ambient sensors. As a result, the combination of ambient sensors and statistical learning algorithms allows for accurate solutions to both the mentioned monitoring and security problems. Although traditionally accurate, each sensor modality and each developed system in literature has drawbacks such as privacy intrusion and low light conditions in the case of cameras, expensive hardware and lengthy setup time in the case of multiple sensors deployed, and related energy and health concerns in the case of active ambient sensors and active ambient signals. Towards the development of a system that

is non-intrusive, non-contact, passive, accurate, and cheap, PIR sensors with statistical learning algorithms are applied to meet the needs of long-term monitoring or security solution.

PIR sensors are cheap, non-intrusive, non-contact, commercial-off-the-shelf (COTS) components that are relatively accurate in monitoring and security applications. PIR sensors function through the detection of a change in infrared radiation across its field of view (FoV) which is detected by the internal pyroelectric elements with opposite polarity. As a result, a motionless human subject will generally go undetected by a traditional PIR sensor due to this lack of change in infrared radiation. For an accurate monitoring and security solution, this major known drawback of PIR sensors must be addressed. To combat this major known drawback to PIR sensors, this work introduces two novel systems for stationary human presence detection using a PIR sensor. The first introduced system is a motion induced PIR sensor (MI-PIR), which has shown to be an accurate method for detecting stationary human subjects and various other human monitoring classifications [6]. The second introduced system is a chest motion PIR sensor (CM-PIR), which has also proven to be an accurate method for detecting stationary human subjects and has been extended to biometric authentication of various human subjects [7]. These novel systems are dependent on statistical learning algorithms to learn from the variations in the PIR sensor data.

For both the MI-PIR and CM-PIR system, the optimal statistical learning algorithm must be selected, as there exists numerous types. Statistical learning algorithms consist of machine learning algorithms, which in turn also includes deep learning algorithms. Machine learning specifically refers to a computer's ability to train itself without being explicitly told how to do so, whereas deep learning, on the other hand, is referred to as a type of neural network, which can be defined as software constructions that are modeled after the neurons in the human brain [8]. Some

common machine learning algorithms include support vector machine (SVM), random forest (RF), decision tree (DT), logistic regression (LR), and Gaussian process regression (GPR). In terms of deep learning algorithms, artificial neural networks (ANN), recurrent neural networks (RNN), and convolutional neural networks (CNN) are all commonly utilized. Each of these models are utilized for specific purposes, such as traditionally GPR models are utilized for indoor localization problems, RNNs are used for time-series data, and CNNs are for image recognition. As a result, towards a PIR system for monitoring and security applications, an ANN, RNN, and CNN are developed for accuracy comparison in classification tasks, while a GPR model is utilized for the precise indoor localization regression task in this work.

While both MI-PIR and CM-PIR systems are accurate methods for stationary human presence detection using a single PIR sensor, both systems are also accurate methods for related monitoring and security classifications and regressions. For stationary human presence detection, MI-PIR is shown to be 100% accurate at room occupancy detection for stationary occupied and unoccupied scenarios in an office environment via the rotation of a PIR sensor by a robotic actuator in 36 second complete cycle scans. Further, in an office environment, MI-PIR is shown to be 93% accurate at occupancy count estimation, 95% accurate at relative location classification, and 94% accurate at human target differentiation. In terms of human activity recognition, the MI-PIR system has shown to be 100% accurate at classifying three different activity labels. Towards a monitoring environment more indicative of an elderly monitoring situation, the MI-PIR system was also utilized in a residential environment and showed to be 98% accurate at human activity recognition of six different labels and 98% accurate at relative location classification at four different possible location labels. For precise indoor localization in both ambient locations and with varying subjects included, the model was visually effective at clustering users at their ground truth location, while

providing low level mean squared errors (MSEs). Finally, the CM-PIR system has shown to be 94% accurate at stationary human presence detection and 75% accurate at biometric authentication.

The rest of this thesis is structured as follows. For further mathematical and technical background of some of the key concepts introduced in this thesis, the "Background" section is next. Towards understanding the novelty of the systems introduced in this work, the "Related Work" section highlights those related systems found in literature. The "Motion-Induced Passive Infrared Sensor (MI-PIR)" section presents the MI-PIR system and related classifications and regressions for human monitoring and the "Chest Motion PIR Sensor (CM-PIR)" section presents the CM-PIR system and related classification for monitoring and IoT security applications. The "Discussion" section compares related systems to the proposed systems and the "Conclusion" summarizes the importance of the work.

Background

Towards a greater understanding of some of the key concepts introduced previously in the introduction, this section highlights the functionality of PIR sensors, the physiological background behind heart-related biometrics, and a brief introduction of some of the performance metrics utilized in this work.

PIR Sensors

As stated, PIR sensors detect humans via the change in infrared radiation across its FoV. There exist two types of PIR sensors: digital PIR sensors and analog PIR sensors. Digital PIR sensors output a "1" or "0" in the case of human detected or no human detected, respectively. The human detection classification from these PIR sensors is dependent on a defined, embedded threshold. As a result, with varying conditions such as a variation in ambient temperature or with

another object in motion such as in the case of a ball or an animal, the binary PIR sensor could theoretically be triggered and result in a false positive. In the case of analog PIR sensors, the raw analog voltage values can be extracted and utilized with statistical learning algorithms for more robust and accurate human detection, as well as for related classification and regression tasks. The raw analog output voltage values are represented as a sinusoidal wave in the case of a human walking past a stationary PIR sensor. On the other hand, in terms of MI-PIR, the collected data is represented as continuous waveforms with many sinusoidal swings due to the many inanimate objects and human subjects that cause the continuous triggering of the PIR sensor while in motion. Figure 5 (a) represents the raw voltage of the MI-PIR system in the "Motion-Induced Passive Infrared Sensor (MI-PIR)" section.

Not only does there exist a differentiation between digital and analog PIR sensors, but there also exist a difference between PIR sensors developed by varying manufacturers. This is due to the variations in the Fresnel lens. A Fresnel lens is included with a PIR sensor to expand the FoV of the sensor into many evenly spaced fan-shaped zones with alternating polarities, as well as to focus the thermal image on the internal pyroelectric elements [9], [10]. In both the MI-PIR and CM-PIR systems, we utilize the analog Panasonic AMN24112 PIR sensor with a manufacturer recorded FoV of 93 degrees in the horizontal direction and 110 degrees in the vertical direction. The manufacturer also records a maximum sensing distance of 10 m when utilized as a traditional motion detector. This Panasonic AMN24112 PIR sensor was chosen based on its analog output capabilities and its detailed datasheet of these quantifiable parameters. The outer white shell with the hexagon-like markings presented in Figure 1 is the Fresnel lens included with the Panasonic AMN24112 device.

Figure 1. Panasonic AMN24112 device used in both novel PIR systems introduced in this work

As mentioned, there exist a dependency between the ambient temperature/environment and the human subject in terms of the infrared radiation radiated by the subject. This dependency plays a large role in the proposed CM-PIR design, as the subjects are to be authenticated in a multitude of environments for the biometric authentication classification. The dependency on infrared radiation with the surrounding ambient environment can be explained with (1). In (1), the total power radiated (W_{tot}) is represented by the energy loss ($T^4 - T_s^4$) between a blackbody (T) and its surroundings (T_s) multiplied by the total surface area of the human subject (S) and the Stefan-Boltzmann constant (σ_{SB}) [11]. With (1), the ambient environment dependency is proven.

$$W_{tot} = S\sigma_{SB}(T^4 - T_s^4) \quad (1)$$

Heart-Related Biometrics

Every single human subject has a unique heart due to the varying sizes and shapes of each heart and due to the variations in opening and closing of the valves that exist within a heart. The traditional method for extracting heart-related information in a clinical setting is the electrocardiogram (ECG), which is a measurement of the electrical activity of the heart. An ECG is generally dependent on surface electrodes for the accurate capturing of the waveforms. The waveforms that exist within one heartbeat include the P, Q, R, S, and T waves, all of which have

unique shapes on an ECG waveform [11], [12]. Each wave represents a unique repolarization or depolarization of a specific part of the heart muscle and the QRS waveform is often utilized for the biometric identification systems in literature, as this is often the most indicative feature of unique individuals. Many of the current systems in literature for heart-related biometric identification utilize this unique waveform with statistical learning algorithms to learn the slight variations that exist within these ECG signal waveforms. Due to ECG signals being dependent on surface electrodes, there does exist a need for a more suitable long-term solution that utilizes a non-contact system for extracting the heart-related information.

There does exist various systems that claim to be non-contact methods for recording the ECG signal, yet none of which are exactly ambient in nature. For example, ECG signals can now be captured via commercial wearable devices as with the release of the Apple Watch Series 5, but this methodology still requires contact with the end user. Further, ECG signals been collected via capacitive coupled electrodes embedded within clothing, which requires contact with the human subject [13]. Although the proposed approach in this work for extracting heart-related information is not as informative and of high resolution as a clinical-grade ECG signal, the signal obtained with the CM-PIR system provides adequate initial results for the biometric authentication classification.

Performance Metrics

Statistical learning algorithms suffer from the black-box stigma as supervised learning models are fed input data with ground truth labels and subsequently produce results based on patterns learned by the machine. To help alleviate this stigma, proper reporting of the performance is paramount. Reporting of the performance of statistical learning algorithms varies based on the

model and the type of classification or regression at hand. To properly highlight the performance of the statistical learning algorithms utilized in this work, the performance is characterized by the accuracy, classification reports, confusion matrices, and visual representations. With that, we also utilize the "Explainx" library in the Python programming language with the explainx.ai function to briefly highlight the importance of features of the CM-PIR sensor data. This library refers to the field of Explainable AI, which is a growing field to adequately explain and represent the performance of statistical learning models [14], [15].

For the GPR model utilized for precise indoor localization with the MI-PIR system developed in this work, we present the mean squared error (MSE) for performance reporting. GPR models are defined as probabilistic supervised machine learning frameworks that incorporate prior knowledge for regression and classification tasks and the performance of these models are quantified by the MSE, which is presented in (2) [11], [16]. y_j refers to the observed values, $y(x_j)$ refers to the predicted values, and N is the number of data points in the training set [11].

$$MSE = \frac{1}{N}\sum_{j=1}^{N}(y_j - y(x_j))^2 \quad (2)$$

Related Work

Towards emphasizing the importance of both the MI-PIR and CM-PIR systems, a brief introduction of various other systems proposed in literature will be presented. Related work on combatting the stationary human presence detection issue with one PIR sensor will be highlighted first. Towards the comparison of existing monitoring solutions, selected systems with various ambient sensors and signals will also be presented. Likewise, solutions utilizing GPR models for the precise indoor localization of human subjects are included. Finally, solutions for biometric authentication and identification will be highlighted in the last portion of this section.

PIR Sensors

As addressed, PIR sensors are known to be unreliable sensors for stationary human subjects as they rely on a change in infrared radiation for detection. Two different research groups have developed novel systems to address this problem and increase the potential applications for PIR sensors [17]–[19]. Both novel systems are based on an optical shutter, which is used to periodically chop the FoV of the PIR sensor that is needed for accurate stationary human presence detection. In [17], the authors developed the initial work for such a device, showing 100% accuracy at stationary human presence detection at a maximum sensing distance of 7 m and a recorded horizontal FoV of 110 degrees. In [18], the authors most recently optimized their optical shutter approach and presented the *SLEEPIR* system, which utilizes one PIR sensor and a novel optical shutter design towards a more energy efficient method of stationary human presence detection using one PIR sensor.

PIR sensors have also been utilized in various monitoring solutions presented in related literature, yet many of these systems are reliant on the deployment of multiple PIR sensors for accurate human position tracking in an indoor environment or are reliant on sensor fusion for accurate detection during sedentary moments. For example, in [20], the monitored user is proposed to wear an inertial measurement unit (IMU) around their thigh capturing the acceleration and angular rate of the human subject, while the eight PIR sensors capture the trajectory of the subject via the binary output of each of the sensors. A similar system can be identified in [21], where a CNN was utilized for early detection of dementia by classifying travel patterns in an at-home environment. These travel patterns are captured by numerous binary PIR sensors deployed throughout the home environment. In terms of human activity recognition systems, two PIR

sensors were deployed in the *ALPAS* system to recognize sedentary activities performed on a couch in at-home environment, showing a final F-measure of 57% [22].

Human Monitoring

Towards a comparison of PIR sensors and other sensor modalities, various systems that are reliant on ambient sensors and statistical learning algorithms have been proposed in literature and are now introduced in this section. Each sensor modality has advantages and disadvantages that makes their deployment more advantageous than others for the problem at hand. For example, in [23], multiple microwave sensors and a 3D-CNN were utilized for accurate multi-person activity recognition with the novelty of the system lying in their developed loss function for weakly-supervised multi-labeled learning. In [24], thermal sensors were deployed with machine learning algorithms, showing 97.5% accuracy for activity recognition. Image sensors and optical sensors were deployed throughout a large exhibition hall, including at the entrances and exits, in another related work. Utilizing an RNN with LSTM units to solve the vanishing gradient issue, the proposed system was accurate at occupancy count classification for respective zones in the exhibition hall [25].

Although there exist numerous systems using ambient sensors for human monitoring purposes, there also exist many systems that leverage ambient signals for human monitoring classification and regression purposes. Novel research completed by the MIT CSAIL research group has shown the efficacy of using active RF signals for locating individuals and recognizing activities performed by human subjects even through walls and occlusions [26]–[28]. In contrast, utilizing passive RF signals is of lower resolution, but is more advantageous due to decreased energy usage and lower health-related concerns. Work has been conducted in our research group to leverage passive RF signals for human detection both in indoor environments and in vehicles

[29]. This work uses principal component analysis (PCA) for dimensionality reduction, recursive feature elimination with logistic regression (RFE-LR), and machine learning algorithms for accurate human detection. Included in ambient signals for human monitoring applications is those systems that leverage Wi-Fi CSI. In [30], a novel deep learning algorithm coined AE-LRCN was used to learn from the variations in Wi-Fi CSI for a 97.6% accurate human activity recognition classification.

GPR models are often applied to precise indoor localization regression problems with ambient sensor modalities or ambient signals. Where the distinct classification of the location of a human subject in an indoor environment proves effective, regression of the precise indoor localization via a regression model can predict the user's location in a continuous fashion, which is more beneficial in a non-contact continuous monitoring application. In [31], a novel indoor localization approach coined *DeepMap* is proposed, for which the namesake refers to the deep Gaussian process for indoor radio map construction and indoor localization estimation via the received signal strength (RSS) of Wi-Fi signals. Likewise, a similar work has been proposed in [32], for which the proposed system leverages the received signal strength indicator (RSSI) fingerprinting data with a CNN to learn the features before the GPR estimates the locations of the human subjects. This hybrid model of applying both the CNN and GPR model to the location data has shown to improve the k-nearest neighbor (k-NN) approach in literature by 68.1%. Lastly, our research group has proposed a system using the GPR model to model the Wi-Fi RSS feature dataset. This work utilizes the GPR model as an initial pose estimation for the portable 3D visual sensor based indoor localization system developed on an iOS device [33].

Biometrics

Classifications using biometric qualities correspond to biometric authentication and biometric identification. As introduced, the ECG signal is a popular state-of-the-art technique for biometric identification using a heart-related feature signal. In [34], an automatic identification system utilizing a CNN deep learning model and the ECG signal data from the MIT-BIH database was developed to eliminate the time-extensive feature engineering process that is related to these biometric identification systems. Moreover, because the unique identifier in ECG signal data is the QRS complex, a QRS resampling strategy based on the PCANet deep learning architecture is applied to handle variations in heart rates due to exercise and other non-sedentary activities [35]. This methodology proved 94.4% accurate at identification on only five heartbeats from the ECG-ID public database. In [36], a cascaded CNN model including F-CNN for feature extraction and M-CNN for identification is applied to ECG signal data showing 97.1% accuracy for biometric identification on ten seconds of heartbeat data. Although these approaches are highly accurate at biometric identification, access to clinical ECG data is limited or non-existent in a long-term IoT security system.

Due to the reduced resolution with the current implementations of ambient sensors or signals for heart-related biometrics, the classification is generally altered to biometric authentication in these instances. With that, towards a non-contact and cheap biometric authentication system for long-term and continuous monitoring, various systems have been proposed in literature. For example, a PPG-based biometric authentication system that relies on facial features from videos is proposed in [37]. This proposed method achieves an average authentication accuracy of 86.67% via the extraction of the cardiovascular based feature using the Laplacian pyramid signal processing technique. In terms of a radar-based approach for

authentication, in [38], a microwave Doppler radar is applied for respiration-related biometric authentication as the phase change of the reflected signal from the chest is related to the cardio-respiratory activity of the human subject. A SVM machine learning model is applied to this microwave Doppler radar data for 100% accuracy at authentication of six subjects in one ambient environment. A similar system is proposed in [39], for which their system coined *Cardiac Scan* applies a DC-coupled continuous-wave radar for authentication of a dataset consisting of 78 subjects in one ambient environment. The results of this work show 98.61% accuracy at authentication while applying the SVM machine learning model. The proposed systems in [38], [39], as well as various other radar-based non-contact authentication systems based on heart-related and respiration-related biometric features, are compared in [40].

These proposed radar-based systems introduced above are active systems that raise health and energy concerns for a long-term monitoring solution. For a modality that is non-contact, cheap, and passive, one would identify a PIR sensor to fit these necessary qualifications. In [41], the authors propose a PIR sensor for resting heart rate estimation using a novel acceleration filter, which is based on computing the second derivative of the raw voltage PIR sensor data with a convolving triangular window and simple Lagrange low pass filter. The second derivative allows for extraction of the low magnitude heart rate in relation to the respiration signal from the PIR voltage data. This novel acceleration filter is introduced in (3). Due to the efficacy of the approach in this reference, we apply a similar methodology of data collection in the CM-PIR system, as well as apply this novel acceleration filter to the CM-PIR system data introduced in this work.

$$g'_2 = [1\ 4\ 4\ -4\ -4\ -10\ -4\ 4\ 4\ 1] \tag{3}$$

Motion Induced Passive Infrared Sensor (MI-PIR)

For both a PIR sensor solution that can solve the stationary human presence detection problem, as well as for a long-term elderly monitoring solution that is cheap, passive, and non-contact, a motion-induced PIR sensor (MI-PIR) system is developed [6]. The MI-PIR system artificially induces the change in infrared radiation needed for accurate detection of stationary human subjects by rotation of an analog PIR sensor by a robotic actuator. Figure 2 presents the complete set-up of the MI-PIR system. MI-PIR consists of the Panasonic AMN24112 PIR sensor, a Dynamixel MX-28 robotic actuator, a Hokuyo UTM-30LX-EW platform, a cardboard thermal insulator, an Elegoo Uno R3 microcontroller, and a PC.

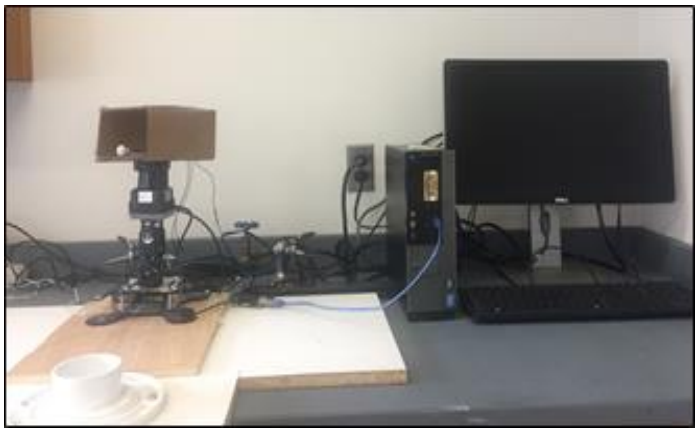

Figure 2. The full MI-PIR design with a PIR sensor, actuator, platform, thermal insulator, microcontroller, and PC.

The robotic actuator rotates the PIR sensor in a 26 second forward scan and a 10 second backward scan for the completion of an entire 36 second scan of the indoor environment. The platform introduced serves no other purpose in the design but to provide a flat surface for the thermal insulator to rest. The cardboard thermal insulator, on the other hand, serves to block any nearby infrared radiation resulting from the rotation of the robotic actuator. Worth noting, a more long-term insulating material will be introduced in a later design; however, the cardboard insulating material is an adequate material to block the nearby infrared radiation in this initial

design. The Elegoo Uno R3 microcontroller is a cheap, COTS device utilized in the design for communication and data conversion between the sensor and the PC. Finally, the PC collects the data in the Arduino integrated development environment (IDE) for future data pre-processing.

The MI-PIR system not only addresses the stationary human presence detection problem with PIR sensors, but also expands the applications of a PIR sensor to various human monitoring classifications and regressions. For the initial data collection in an office location, MI-PIR shows high accuracy at occupancy classification, occupancy count estimation, distinct location classification, human target differentiation, and human activity recognition. In addition, the GPR model is applied to the data collection in this office environment and shows the effective ability to cluster locations of many users, as well as with data from only one subject. To simulate an environment more representative of an elderly monitoring situation, data is collected in a residential apartment environment for classification of both distinct locations and human activity recognition with high accuracy. The GPR model is also applied to this dataset to estimate the location of an individual based on the performed activity in the residential environment. This section will highlight these reported accuracies through the presentation of the data collection, data pre-processing, classification and regressions, and the optimization and quantification of the MI-PIR system.

Data Acquisition

For data acquisition, the MI-PIR system scans an entire ambient environment in 36 second cycles with a 130-degree motion at a 10 Hz sampling rate. With that, the MI-PIR system design increases the FoV of the Panasonic AMN24112 PIR sensor from 93 degrees to 223 degrees. As mentioned, there exist two different environments for data collection: an office environment and a residential environment. Each PIR raw voltage data sample from each ambient environment is

captured by Student 1 of Tables 1 and 2, who runs and ensures the data collection is captured properly. Table 1 and 2 highlight the data collection for each classification and regression completed in the office environment and the residential environment, respectively. These tables include the classification, the integer label used for the supervised statistical learning algorithms, the real label, and the number of 36 second samples collected for. The coordinate systems for each table represent the precise indoor localization approach to predict the coordinates of the human subject in the ambient environment. In terms of the full data collection for indoor localization in Table 1, three coordinates are fed to the GPR model to ensure equal lengths between each input. For example, a sample with three individuals at Locations 3 through 5 would contain the coordinates "(250, 265), (80, 265), (50, 60)", while a sample with only one individual present would contain padded unoccupied coordinates. The latter example can be represented by the situation where only one human subject is present in the office environment at Location 1, which is subsequently provided the ground truth coordinate system of "(415, 70), (250, 10), (250, 10)". The unoccupied coordinate systems for both ambient environments are given a ground truth coordinate system near the entrance of the environment to not interfere with any other location samples that are close in proximity. Those classifications or regressions that only include Subject 1 for the office environment in Table 1 are labeled as such, whereas all classifications and regressions in Table 2 are completed by Subject 1 only.

In terms of data acquisition, each collected data sample is synced to match the ambient environment e.g., each data sample starts at the farthest left point of the scan. For any change of state occurring in the ambient environment, such as a human subject changing states from sitting to standing or any new individual entering the room, the data collection period will halt, and a new data collection sample will begin when the new state remains constant. For unoccupied scenarios,

Subject 1 remains outside of the ambient environment and appends 36 seconds to the start of the data sample to ensure adequate time to leave the room location. For occupied datasets, a remote desktop is used with the PC that communicates with the MI-PIR system to record the exact time for which the PIR sensor is at the farthest left position. Each data sample is copied from the serial monitor of the Arduino IDE and then converted to CSV format, where the data is cleaned and manually labeled. After this manual process, each data sample is then sent to their respective folder for future classification or regression within the Jupyter notebook.

Table 1. MI-PIR data collection in the office space location.

Occupancy Parameter	Number Label	Real Label	Available Samples
Room Classification	0	Unoccupied	854
	1	Occupied	2803
Occupancy Count Estimation	0	No People	854
	1	One Person	1936
	2	Two People	702
	3	Three People	165
Relative Location Classification	0	Unoccupied	854
	1	Location 1	174
	2	Location 2	1240
	3	Location 3	153
	4	Location 4	369
	6	Locations 1 and 2	105
	10	Locations 2 and 3	44
	11	Locations 2 and 4	100
	12	Locations 2 and 5	250
	15	Locations 4 and 5	203
	23	Locations 2, 3, and 5	138
	24	Locations 3, 4, and 5	21
	25	Locations 2, 4, and 5	6
Human Target Differentiation	0	Unoccupied	854
	1	Student 1	1936
	2	Students 1 and 2	32
	3	Students 1 and 3	181
	4	Students 1 and 4	386
	5	Students 1 and 5	103
	6	Students 1, 4, and 5	98
	7	Students 1, 3, and 5	46
	8	Students 1, 4, and 6	21
Indoor Localization	(250, 10)	Unoccupied	7136
	(415, 70)	Location 1	279
	(415, 265)	Location 2	1883
	(250, 265)	Location 3	356
	(80, 265)	Location 4	699
	(50, 60)	Location 5	618
Indoor Localization – Student 1	(250, 10)	Unoccupied	0
	(415, 70)	Location 1	174
	(415, 265)	Location 2	483
	(250, 265)	Location 3	153
	(80, 265)	Location 4	369
	(50, 60)	Location 5	0
Activity Recognition – Student 1	0	Unoccupied	191
	1	Sitting	102
	2	Walking	101

Table 2. Data collection for the MI-PIR system in a residential environment.

Occupancy Parameter	Number Label	Real Label	Available Samples
Relative Location Classification	0	Unoccupied	185
	1	Location 1	370
	2	Location 2	208
	3	Location 3	384
Indoor Localization	(425, 50)	Unoccupied	185
	(290, 260)	Working at Desk	208
	(225, 150)	Laying on Ground	186
	(200, 150)	Exercise on Ground	184
	(125, 260)	Watch TV on Bed	174
	(100, 270)	Sleep on Bed	210
Activity Recognition	0	Unoccupied	185
	1	Working at Desk	208
	2	Laying on Ground	186
	3	Exercise on Ground	184
	4	Watch TV on Bed	174
	5	Sleep on Bed	210

Office Environment

The office environment used for data collection is modeled in Figure 3. The office environment is an academic office location with five different desk locations, each of which are accompanied by a desktop and a PC. The occupants of this office location are only those student researchers with key access, and for which all such occupants agreed to be monitored but are not actually aware of when the monitoring occurs. This discrete monitoring process ensures that the data collection is representative of a true work environment, and the occupants are in their normal and true stationary state.

The five PC locations in the office environment are labeled as “Location (L1)” through “Location 5 (L5)” on Figure 3, where the MI-PIR system is placed for data collection at Location 1 for the highest vantage point. These locations are referenced in Table 1 as the locations of student researchers for both distinct location classification and precise indoor localization regression. The office location is 5.18 m in length and 3.96 m in width, and as a result the precise indoor localization coordinates are modeled in cm to match these measured values. For the “walking”

label in the activity recognition classification of Table 1, Subject 1 paces in three pre-defined walking paths ("W1-W3") as labeled in Figure 3.

Office data collection for stationary human presence detection, occupancy count estimation, relative location classification, and human target differentiation was completed between August to December of 2019. This covered the change in the summer semester to the fall semester on campus, allowing for variations in the student researchers and their usual locations in the office environment. In addition, the ambient environment in the data collection varied due to the sunlight changes between seasons that existed with the open windows in the office. These changes between locations and ambient environments allow for a more robust monitoring system. Precise indoor localization via GPR is based on the same data collection; however, data collection for the "walking" label of activity recognition was collected in March by Student 1 only. Activity recognition in this office environment is completed with Student 1 only as well, and precise indoor localization is presented with a Student 1 only model and with a full data collection model.

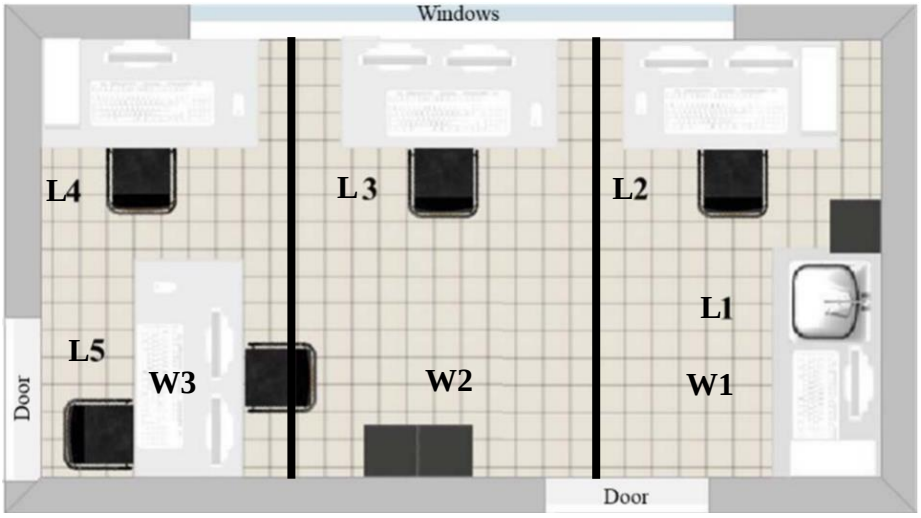

Figure 3. The model of the office environment. "L1" through "L5" indicate the five stationary locations in the office space and "W1" through "W3" indicate the three walking paths during the HAR data collection. MI-PIR is located on the counter at L1.

Residential Environment

The residential environment utilized for data collection in Table 2 is modeled in Figure 4. The residential environment is an apartment bedroom that is 4.57 m in length and 3.65 m in width, and as a result, the precise indoor localization coordinates are also provided in cm to match these measured values. The locations for which each activity is completed is provided in Figure 4 and labeled as Location 1 ("L1") through Location 3 ("L3"). The locations are not provided the coordinate system for precise indoor localization in this ambient environment, as the activities differentiated slightly at the distinct location. For examples, "A2" and "A3" were both completed at the distinct location of "L1", but the two activities differentiated slightly in location for precise indoor localization. The five different activities completed in this location for the activity recognition classification are also labeled in Figure 4, respective to the locations for which they were performed at. Location 1 corresponds to an empty carpet space for which Subject 1 performs "Laying on Ground (A2)" and "Exercise on Ground (A3)". The "Laying on Ground" activity, for which Subject 1 laid on the ground motionless for a continuous period, corresponds to a potential fall event that an elderly individual may suffer from. This activity relates to an elderly monitoring situation, as a fall event is the most important label to classify for elderly monitoring systems [42], [43]. Moreover, Location 2 is the desk location for which Activity 1 ("A1") of "Working at Desk" is performed. Figure 4 specifically presents the instance of "A1" being completed at "L2", indicated by the modeled human working at the desk location. Lastly, Location 3 corresponds to "Watch TV on Bed (A4)" and "Sleep on Bed (A5)". Performing multiple activities at the same location allows for the classification of activities to be more robust, as the statistical learning model is learning from the different activities and not just the different locations.

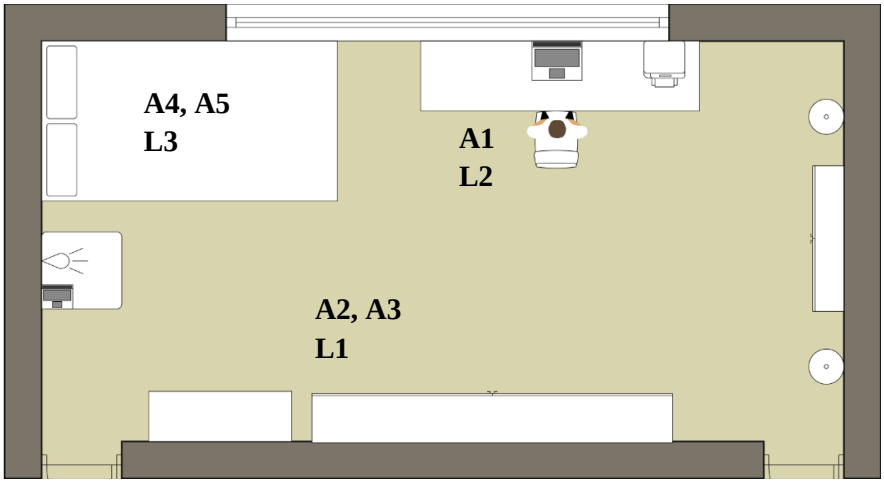

Figure 4. Model of residential environment data collection. MI-PIR is located next to the bed, indicated by the outward signals on the side table.

Overall, Student 1 was the only human subject utilized for data collection in the apartment residential environment. As Student 1 is the only occupant for data collection, the subject knows data collection is ongoing in this case. Moreover, like that of the office environment, continuous data samples are collected for until Subject 1 changes the data collection state, such as with the completion of a given activity. With all the activities in the dataset for the residential environment being completed continuously, each of the activity samples are roughly two hours of data with at most three continuous data samples for each activity present in the dataset.

Data Pre-Processing

Once the data collected in both ambient environments is sent to their respective folders, the entire dataset can then be pre-processed in each respective Jupyter Notebook file utilizing the Python programming language. The “read_csv” function of Python reads the data and batches all data samples together. To increase the number of data samples and to allow for quicker classification times, continuous data samples were batched into 360 second samples based on the time data included in the CSV file. This 360 second sample accounts for the 36 seconds to complete

one full scan and the 10 Hz sampling rate used for data collection. The classifications and regressions are based off this 360 second batch rather than a large continuous data file of varying sizes. Towards a feature that is representative of the numerous classifications and regressions utilized with the MI-PIR system, a feature engineering process is completed and is based off these 360 second batches.

Fourier transforms are popular in signal processing domains and they relate the captured time-series data to the frequency spectrum [44]. Presented in (4) below is the function utilized for the calculation of the Fourier transform from $f(t)$, the time-series representation of the function. In Python and with other programming languages, the fast Fourier transform (FFT) is a particularly helpful function that calculates the coefficients of the signal in an efficient manner. For the MI-PIR time-series batches, we calculate the FFT coefficients and take the absolute value providing the signal power of each batch.

$$F(w) = \int_{-\infty}^{\infty} f(t) e^{-jwt} dt \tag{4}$$

The signal power was hypothesized to be a strong indicator of human presence due to the varying ambient conditions that exist within the dataset and this hypothesis proved true not only for room occupancy classification but for each other classification and regression completed with the MI-PIR system. Figure 5 (a) presents the raw analog PIR voltage data for the stationary human presence detection classification of an occupied scenario against an unoccupied scenario and Figure 5 (b) presents the signal power of the same data. Figure 5 illustrates the visual differences identified between the raw voltage and the calculated signal power, while also illuminating the reason for its success with the statistical learning algorithms, as the pattern identified with the

signal power representation (the occupied data showing greater signal power than unoccupied data) is consistent among many different samples.

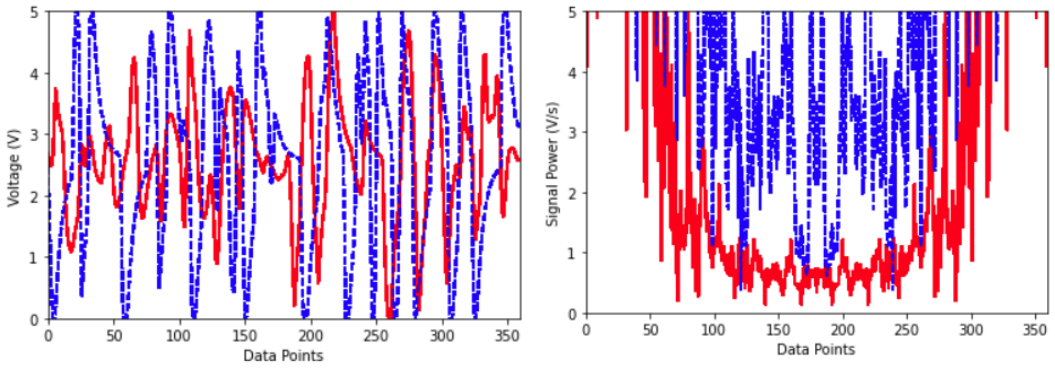

(a) (b)

Figure 5. MI-PIR data represented as the (a) raw voltage data and (b) signal power calculated with the FFT, with the occupied scenario in dashed blue and an unoccupied scenario in solid red.

The final steps that are required in the data pre-processing stage before being fed to the statistical learning algorithms for classification is normalization and the splitting of the data. With the sklearn min max normalization function, the signal power features are normalized from zero to one for greater classification and regression performance. Some of the models, however, performed better with the raw signal power values. These include the maximum sensing distance classification and the GPR models. Otherwise, the signal power was normalized for classification purposes. Furthermore, the MI-PIR sensor data is split between 70%, 15%, and 15% for training, testing, and validation purposes for each model, respectively. For example, with all the available data collected for in each of the first four classifications (room classification, occupancy count estimation, distinct location classification, and human target differentiation), there exist 3,657 samples that is then split amongst the training, testing, and validation sets. The overall data of each classification and regression can be added up for each classification or regression row in Table 1 and Table 2. The training data is then utilized in the training of the statistical learning algorithms and the testing data is utilized for performance analysis of the models.

Statistical Learning

Three deep learning algorithms were developed towards a comparison of the most optimal model, determined through a comparison of reported accuracy from each of the various classifications completed in the office environment. The determined optimal deep learning model will then subsequently be applied to the residential environment classifications. On the other hand, one machine learning algorithm was developed for precise indoor localization with the MI-PIR sensor data. An ANN, RNN with LSTM units, and a CNN were all developed for classification and a GPR was developed for a regression of the precise indoor localization of the human subjects. The deep learning models were built with the Keras library and the GPR model was built with the sklearn package in Python.

Figure 6 presents the architectures utilized for each deep learning model in the office environment activity recognition. These model architectures are highly similar across all the classifications completed in the office environment, with adjustments in loss functions and optimizers depending on the number of outputs required. Further, epochs are generally similar across each model, with slight deviations resulting due to different classifications. Figure 6 (a) presents the ANN architecture utilized for the office environment activity recognition. The ANN is composed of one input layer, one hidden layer, and one output layer for classification of three activities. This specific implementation of the ANN model utilizes the Adam optimizer, sparse categorical crossentropy loss function, rectified linear unit (ReLu) activation functions, and softmax output activation function. 200 epochs were utilized for training with this developed ANN deep learning model. Moreover, the RNN architecture presented in Figure 6 (b) is composed of two long short-term memory units (LSTM), two dense layers, and three dropout layers to help with overfitting. This RNN uses the same loss functions and activation functions as the ANN, with the

only change being the number of epochs, which was reduced to 100. Finally, the CNN presented in Figure 6 (c) is composed of two convolutional layers, one dropout layer, one max pooling layer, one flattening layer, and two dense layers. The developed CNN deep learning model is also composed of the same loss functions and optimizer as the other two deep learning models. The CNN is trained with 10 epochs.

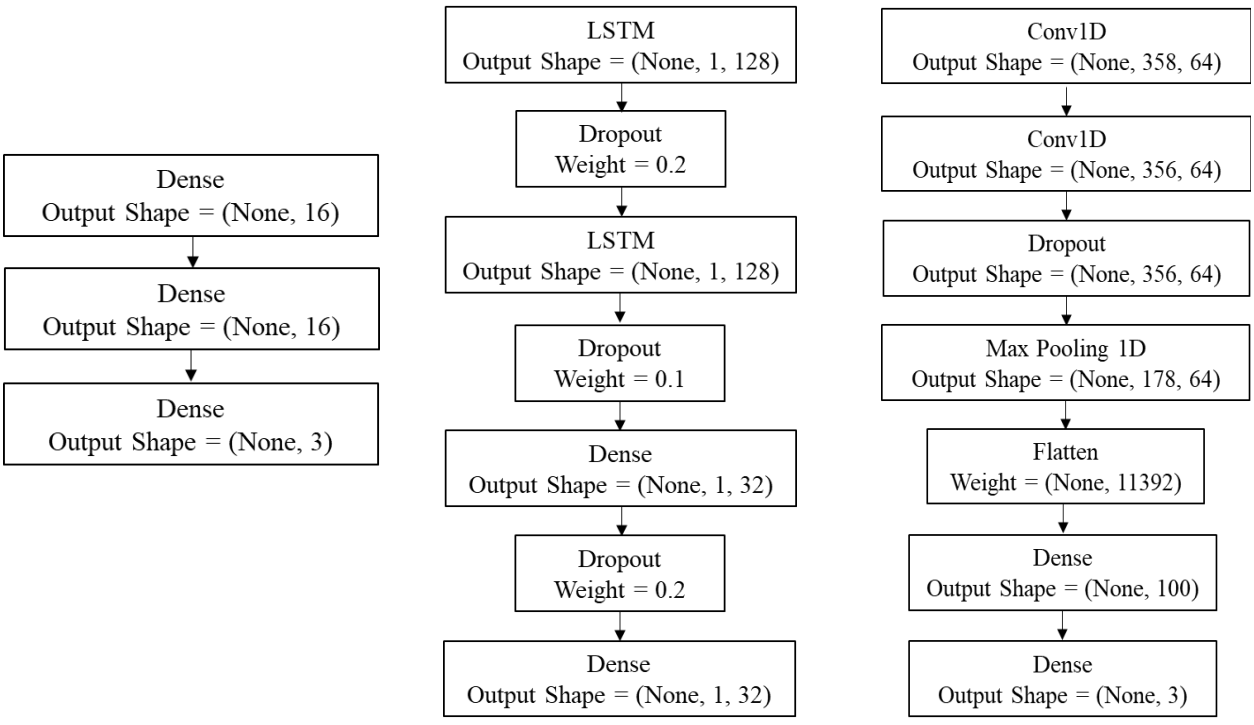

Figure 6. The three deep learning model architectures utilized for the office space activity recognition with (a) the ANN, (b) the RNN with LSTM units, and (c) the CNN.

The accuracy comparison of the three different deep learning models deployed for classification in the office environment is presented below in Table 3. The greatest classification accuracy amongst the three different models is the RNN deep learning model. All three models performed well on the MI-PIR sensor data for all five classifications, with the RNN with LSTM units performing slightly better as hypothesized due to the time-series nature of the data. A

complexity analysis of each architecture is needed for a more accurate comparison. With that, each model can be theoretically optimized and fine-tuned to enhance the results of each classification.

Table 3. Office environment classification comparison of three different deep learning models implemented.

Model:	Room Classification (%)	Occupancy Count (%)	Location Classification (%)	Human Target Differentiation (%)	Office Activity Recognition (%)
ANN	99	91	93	93	100
RNN	100	93	95	94	100
CNN	100	90	93	94	100

For the precise indoor localization regression problem in both the office environment and the residential environment, a GPR model is developed and applied to the MI-PIR system data. The GPR model utilized for precise indoor localization is developed with the sklearn package in Python. The MSE output of the GPR model was compared with three different kernels: Matern, RBF, and ExpSineSquared. The Matern kernel showed the best result and is thus utilized for the precise indoor localization regression problems in this work.

Classifications

Table 3 highlights the various classifications and the accuracies obtained by applying the three different deep learning models. With the RNN model with LSTM units found to be the optimal deep learning framework, the presentation and analysis of those classifications will correspond to the RNN model. Asa a result of the RNN model being the optimal deep learning framework via the comparison analysis, the RNN model will be applied to the classifications completed in the residential ambient environment.

The office environment consists of five different classifications: room occupancy classification, occupancy count estimation, distinct location classification, human target differentiation, and activity recognition. The room occupancy classification achieved 100%

accuracy with the RNN model, proving that the MI-PIR system can accurately detect stationary human occupants every 36 seconds. With 93% accuracy, the RNN model achieved high accuracy at differentiating the number of occupants in the office space between zero to three individuals, indicating a potential application in a monitoring situation. Further, with 95% accuracy, the MI-PIR system and the RNN deep learning model is an accurate methodology for classifying various integer labels corresponding to unique location combinations of the office occupants. Human target differentiation achieved 94% accuracy at differentiating various combinations of unique users present in the office space, indicating the potential of the signal power feature as a biometric. Finally, with activity recognition in the office space, the model achieved 100% accuracy at differentiating "unoccupied", "sitting", and "walking" activities. Figure 7 (a) presents the confusion matrix for the activity recognition classification in the office space.

Applying the MI-PIR system and the optimal deep learning framework to the residential environment, the accuracies of both distinct location classification and activity recognition are both adequate for a long-term at-home monitoring solution. With the data samples presented in Table 2, the distinct location classification of "unoccupied" to "Location 3" achieved 98% accuracy. Further, the human activity recognition system of recognizing the five activities from "unoccupied" to "Sleep on Bed" achieved 98% accuracy. The high accuracy achieved by the activity recognition classification allows for a monitoring situation where the caregiver or hospital system is aware of the activity being performed by the elderly individual every 36 seconds. This includes a potential fall as collected for with integer label of "2". Figure 7 (b) presents the confusion matrix for the activity recognition classification completed in a residential bedroom. From this confusion matrix, one can identify the greatest confusion occurs with the integer label of "3", but otherwise, the model performed well.

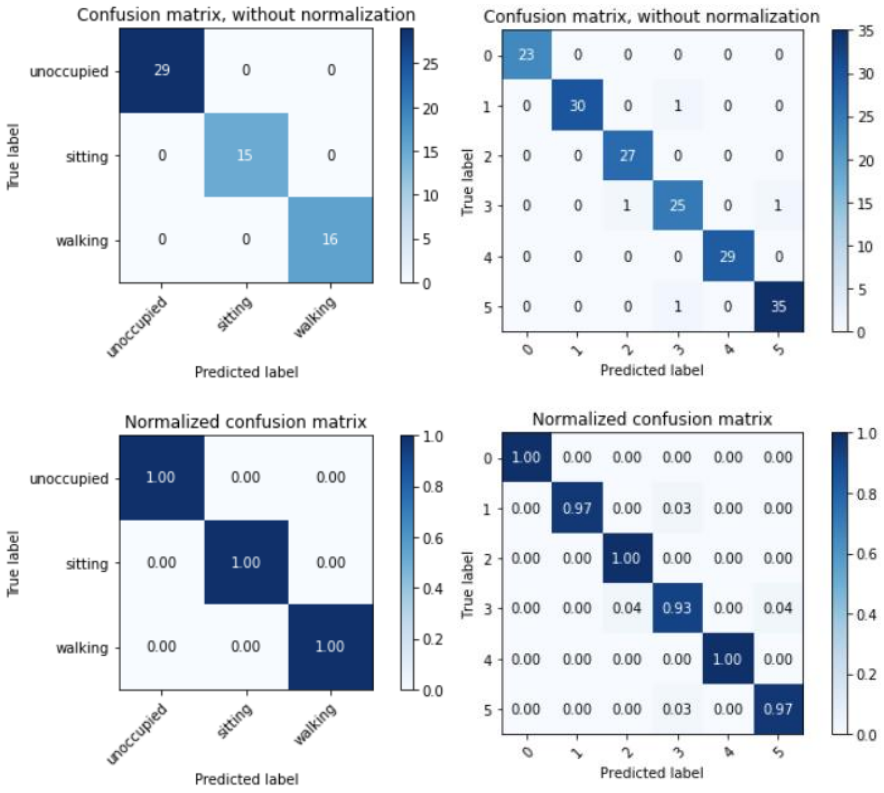

(a) (b)

Figure 7. Confusion matrix of the activity recognition classification completed in (a) the office environment and (b) the residential environment.

Precise Indoor Localization

Although the MI-PIR system is accurate at classifying distinct location combinations in both an office environment and a residential environment, a precise indoor localization system is more adequate for a long-term monitoring situation. The developed GPR model is applied to the data collected in both ambient environments to indicate the applicability of the MI-PIR system for a regression-based localization system. In terms of the office environment, the GPR model is fitted to a scenario of all the data collected and a scenario for which Student 1 is involved only. Comparisons of these models indicate the robustness of the GPR model with MI-PIR system data to cluster locations of human subjects with varying ambient conditions and human subjects present. The second model proves that the GPR model is better with only one subject to be

localized, as indicated by the decrease in the MSE. For the office precise indoor localization model composed of all the stationary data collected within this environment, the model achieved a MSE of 493.7 cm^2. For the office precise indoor localization model composed of Student 1 data only, the model achieved a MSE of 340.8 cm^2. Figure 8 (a) presents the full data collection results from the GPR model and Figure 8 (b) presents the Student 1 only model.

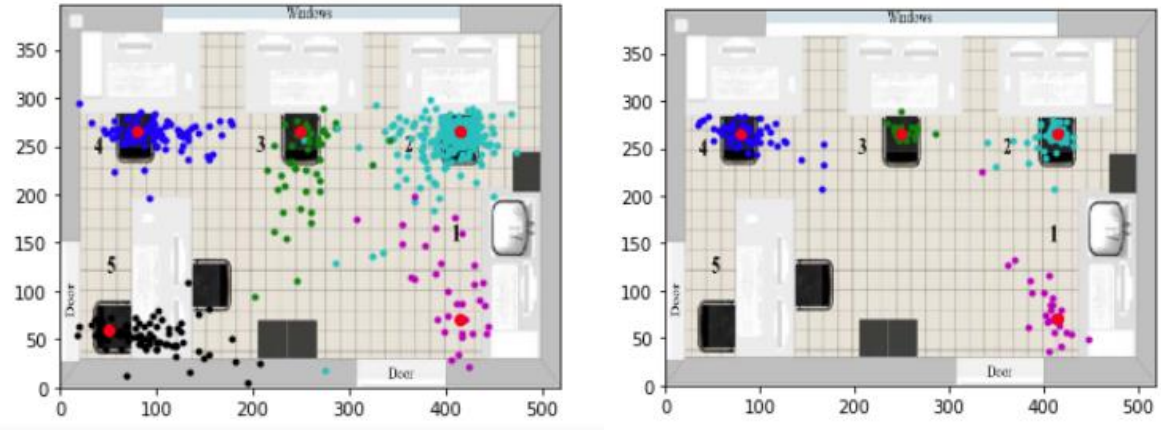

(a) (b)

Figure 8. GPR model results of the precise indoor localization regression approach for (a) all data and (b) Student 1 only.

Figure 8 proves that the GPR model is effective at clustering the locations of various human subjects in Figure 8 (a) and in the case of only one subject in Figure 8 (b) as indicated by the unique colors present at each individual location. During the data acquisition stage, a precise coordinate system is not provided for each unique data sample, as human subjects are free to work at any specific spot at the desk location. A precise ground truth label is hypothesized to increase the accuracy of the model, which subsequently would decrease the MSE, proving to be a more accurate model. Figure 8 (a) also does not provide the clustering of the unoccupied scenarios included in the model, for which these scenarios provide a cluster near the door. The unoccupied scenarios also add to the higher-than-expected MSE. The clustering of distinct locations presented in Figure

8 is evidence enough that the GPR model was successful at precise indoor localization with the MI-PIR system data.

In terms of the residential environment precise indoor localization with the developed GPR model, Figure 9 presents the clustering results of Subject 1 performing various activities. The activities served as the ground truth for the precise indoor localization system as the location of the activities performed by Subject 1 differentiated slightly at each district location. Figure 9 indicates the success of the GPR model at clustering the precise locations of these activities, achieving a MSE of 131.4 cm^2. The yellow cluster near the bottom right of the image is a cluster of unoccupied data collected in the residential environment. This approach, in conclusion, allows for a caregiver or hospital system to precisely identify the location of an elderly individual in an accurate and passive manner.

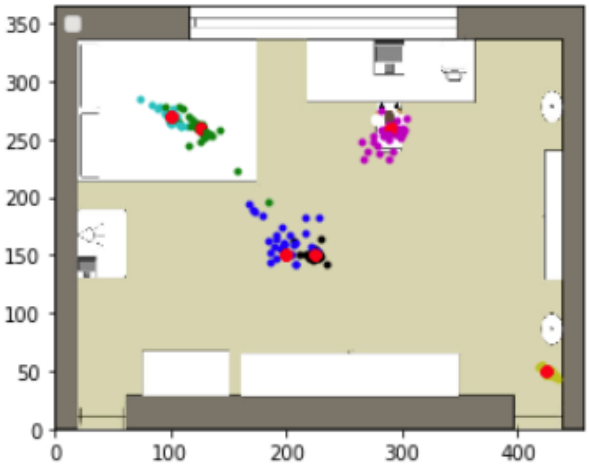

Figure 9. The GPR model results for the precise indoor localization of Student 1 in a residential environment.

System Quantifications

Towards a more accurate comparison of the MI-PIR system with existing solutions to the stationary human presence detection problem using a single PIR sensor, experimental optimization

analysis is completed to analyze the MI-PIR system further. This analysis includes quantifying the optimal rotation time and the maximum sensing distance of the MI-PIR system. Towards this end, the optimal rotation time is determined with varying window sizes completed in the data pre-processing stage and the maximum sensing distance quantification is completed with a new data collection sample in three different ambient environments.

The MI-PIR system is composed of a 26 second forward motion and a 10 second backward motion to complete a full 36 second scan time. To find the optimal rotation time towards the fastest classification of indoor occupancy parameters, these three specified rotation times are compared. Within the data pre-processing stage, the first step is to batch data in 36 seconds in Python, which is based on the time manually appended to the CSV files copied from the Arduino IDE. Those files that are not 360 data points in length are deleted from the end of each data sample collected for. Further, for the 26 second analysis, the last 100 data points are deleted from each 360 data point sample. For the 10 second analysis, on the other hand, the first 260 data points are deleted from each 360 data point sample. Thus, this data pre-processing technique allows for the analysis of three different rotation times towards finding the most optimal solution. Table 4 provides the results of the rotation time analysis on the office data classifications, showing a 36 second rotation time to be the most optimal for the MI-PIR system as indicated by the much greater accuracy with this rotation time. Although a 26 second rotation time provides reasonable classification results, the additional ten seconds of rotation time allows for much greater confidence for an at-home monitoring solution. The accuracies reported in Table 4 are provided while utilizing the ANN deep learning model.

Table 4. Optimal rotation time analysis using the office data and the ANN deep learning model.

Time (s):	Room Classification (%)	Occupancy Count (%)	Location Classification (%)	Human Target Differentiation (%)
36	99	91	93	93
26	98	84	84	89
10	75	71	69	80

With the 36 second rotation time verified as the optimal rotation time for the MI-PIR system, the next quantity needed for determination towards a proper analysis of the MI-PIR system is the maximum sensing distance quantification. The manufacturer of the Panasonic AMN24112 lists the maximum sensing distance as 10 m; however, this value is reported for a PIR sensor deployed in the traditional sense and not a system such as the MI-PIR system utilizing deep learning for classification. To compare this listed value with the MI-PIR system, the MI-PIR system's maximum sensing distance is experimentally quantified through the recording and development of a new dataset in three different ambient environments. Additional ambient environments were added as to expand the maximum sensing distance that could be recorded. For example, the first ambient environment is a residential hallway that is 12 m in length. The second ambient environment is a construction warehouse that is presented in Figure 9 (a) and is 19 m in length. Finally, the third ambient environment is a gymnasium and is 43 m in length.

The MI-PIR system is utilized with a moveable cart platform as indicated in Figure 9 (b) for the maximum sensing distance quantification dataset and Student 1 completes the dataset by sitting and pacing at iterative distances away from the system as to compare the maximum sensing distance between a stationary and moving human subject. These iterative distances are presented in Table 5. In addition, unoccupied samples are collected for in each environment with equal number of data samples to ensure balanced data for learning. Due to the time allowance in the gymnasium, only limited data samples are provided in this ambient environment, but much more

systematic data collection is included with the other two ambient environments. Also, for a more systematic data collection approach, only one ambient environment should be utilized to provide a maximum sensing distance quantification that is dependent on only one environment. In this quantification, however, the results are much more robust due to the multiple ambient environments.

(a) (b)

Figure 9. The (a) construction warehouse environment and (b) the MI-PIR system presented on a movable cart platform.

The results of the maximum sensing distance quantification are provided in Table 5 below. In the residential hallway, the MI-PIR system is 100% accurate at detection of a stationary human and a moving individual past the 10 m maximum sensing distance. As a result, the MI-PIR system is shown to increase the maximum sensing distance of the manufacturer stated 10 m. The maximum sensing distance overall is shown to be 41 m for detecting both stationary and moving individuals in the same dataset utilized for deep learning, whereas the maximum sensing distance for stationary and moving individuals alone is found to be 21 m. Thus, for a more precise maximum

sensing distance, more distances should be collected for in the gymnasium environment between the 21 and 41 m measured distances. In addition, as with all deep learning models, the accuracy is dependent on the number of training samples, which may prove the reason for 41 m being the overall maximum sensing distance, as there exists more data in this case. Overall, it can be concluded that the maximum sensing distance is expanded with the MI-PIR system.

Table 5. Maximum sensing results from three different ambient environments

Ambient Environment	Distance (m)	All Data: Accuracy (%)	Motionless: Accuracy (%)	Motion: Accuracy (%)
Residential Hallway	1	100	100	100
	3	100	100	100
	7	100	100	100
	9	100	100	100
	10	100	100	100
	11	100	100	100
	12	100	100	100
Construction Warehouse	13	100	100	100
	14	100	100	100
	15	100	100	100
	16	100	100	100
	17	100	100	100
	18	100	100	100
	19	100	100	100
Gymnasium	21	100	100	100
	41	100	95	98
	43	95	91	95

Visualizations

Understanding the performance of the RNN deep learning model for the various room occupancy classifications relies on the visualization of inputted features. Visualization is an important aspect in explainability of statistical learning algorithms for the reason of alleviating the black-box stigma surrounding these algorithms. Figure 10 presents the signal power plotted against the number of data points included in one 360 data point batch. As the signal power plot for the room classification occupancy parameter was presented earlier in Figure 5, Figure 10 (a) presents the occupancy count estimation, Figure 10 (b) presents the distinct location classification, and Figure 10 (c) presents the human target differentiation classification. These plots use the raw signal power and not the normalized signal power for visualization. However, plotted in Figure 11 is the

signal power normalized for the activity recognition in both environments, where Figure 11 (a) presents the office environment and Figure 11 (b) presents the residential environment. Each plot includes a legend to map the number label or real label with the specific color plotted.

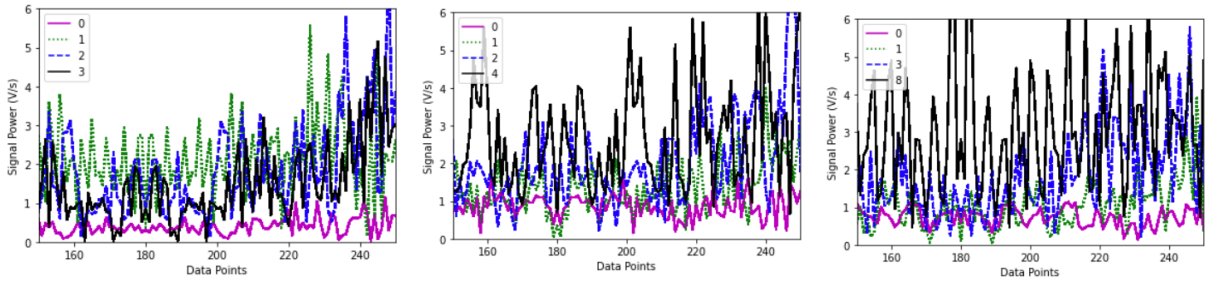

(a) (b) (c)

Figure 10. Raw signal power plotted against the number of data points for the office environment data and for (a) occupancy count estimation, (b) distinct location classification, and (c) human target differentiation.

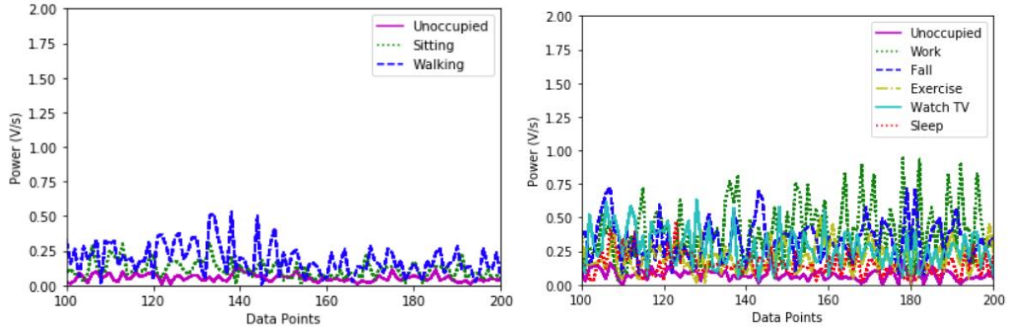

Figure 11. Normalized signal power plotted against the number of data points for the (a) office environment activity recognition and (b) the residential environment activity recognition.

Consistent across all the plots presented in Figure 10 and Figure 11, as well as presented earlier in Figure 5, is the fact that the unoccupied scenario is of the lowest magnitude in each representation. This provides understanding towards the reason behind the MI-PIR system being an accurate system for stationary human presence detection. Comparing those plots that are unnormalized and those that are normalized between zero and one, the normalized plots present similar information at a smaller scale. The normalization allows for the unoccupied scenarios to be mapped closer to a zero magnitude. Further, Figure 10 presents various scenarios for each

classification. For example, the signal power presented in Figure 10 (a) is hypothesized to be of greatest magnitude for the scenario in which three human subjects are present, yet the differences between one subject and three subjects are minimal. Similarly, in Figure 10 (b), with all data being from Subject 1, one would hypothesize that at Location 4 the signal power would be of the lowest magnitude out of the occupied scenarios due to this location being the farthest away from the sensor system, yet this example shows a scenario for which Location 4 has the greatest magnitude. Due to these examples, and because of the changes in human subjects and ambient conditions, the reliance for a deep learning algorithm to learn the slight deviations in these scenarios is paramount to the success of the MI-PIR system. Visualizations of these scenarios show unique time-series signals for each scenario, which can allow for a deep learning algorithm to accurately learn from. The PIR analog voltage data is dependent on ambient conditions, and as represented in Figure 10, various scenarios come into play during training and testing. Moreover, Figure 11 presents scenarios that are consistent with the original hypothesis, for which the "walking" scenario provides the greatest magnitude of signal power in Figure 11 (a) and each activity presents a unique feature that is greater than the unoccupied scenario in Figure 11 (b).

Chest Motion PIR (CM-PIR)

MI-PIR has been proven to be both an accurate method for stationary human presence detection using a single PIR, as well as proven to be an accurate monitoring system via the highly accurate classifications and regressions. MI-PIR, however, requires implementation of additional hardware such as the robotic actuator for the accurate detection of stationary human subjects. Towards presenting a solution for the stationary human presence detection problem with no additional hardware required, a chest motion PIR sensor (CM-PIR) system is presented [7]. CM-PIR is composed of the Panasonic AMN241112 PIR sensor, an Elegoo Uno R3 microcontroller, a

PC, and the optimal RNN deep learning model for both classification of stationary human presence and biometric authentication. The analog PIR sensor of CM-PIR detects the presence of a stationary human subject via the chest motion of the user, as well as classifies one user against all other adversaries based on the unique chest motion for biometric authentication. Figure 12 below presents the CM-PIR system in use for the monitoring of a human subject.

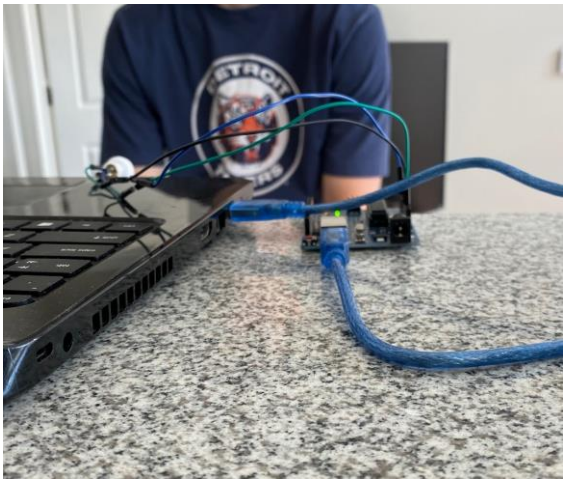

Figure 12. The novel CM-PIR system during the data collection of a human subject.

The CM-PIR system is both a novel system for stationary human presence detection using one PIR sensor and a promising novel security solution for IoT applications. The dataset built for the CM-PIR system is composed of sixteen different human subjects at nine different ambient environments. Utilizing a voltage threshold to ensure the data collected is from the minute chest movements only, four human subjects and three ambient environments are completely removed from the dataset due to both errors with the data and due to continuous movement by the human subject. With this dataset, the RNN deep learning model proves 94% accurate at stationary human presence detection and 75% accurate at biometric authentication. The CM-PIR system will be fully examined through the presentation of the data acquisition, data pre-processing, deep learning, system quantifications, and system visualizations.

Data Acquisition

The data acquisition methodology for collecting the heart-related features of a stationary human subject with an analog PIR sensor is followed from the work presented in [41]. This work utilizes the novel acceleration filter that was previously presented in (3), for which this filter accurately estimates the resting heart rate of individuals using a single PIR sensor. The data in this work is collected at a 1 m distance with a 10 Hz sampling rate, and human subjects are required to sit perfectly motionless away from a PIR sensor that is at chest height from the user. The data acquisition strategy was previously introduced and can be visualized with Figure 12.

Table 6. Complete dataset utilized for the CM-PIR system classifications with a 90 second window size.

Category	Data Collected (Samples)	Data Used (Samples)	Integer Label	Real Label	Location
Stationary Detection	123	122	0	Unoccupied	A-D
	443	295	1	Occupied	A-I
Biometric Authentication	123	122	0	Unoccupied	A-D
	219	133	1	Subject A	A-D
	224	162	2	Adversaries	B, D-I
Individual Subject Distribution	123	122	0	Unoccupied	A - D
	219	133	1	Subject A	A - D
	40	34	2	Subject B	A - C
	19	19	3	Subject C	B
	35	32	4	Subject D	B
	18	14	5	Subject E	E
	9	7	6	Subject F	E
	11	11	7	Subject G	B
	6	0	8	Subject H	F
	14	0	9	Subject I	G
	13	11	10	Subject J	G
	12	6	11	Subject K	B
	7	0	12	Subject L	H
	12	0	13	Subject M	I
	13	11	14	Subject N	F
	12	7	15	Subject O	F
	13	10	16	Subject P	D

Sixteen human subjects volunteered to participate in the CM-PIR data acquisition stage. Towards a robust security system that can differentiate users even in multiple ambient environments, nine different home locations are collected for during data acquisition. Table 6 presents the dataset collected for across sixteen different human subjects in nine different home

environments. The human subjects included in Table 6 are of varying ages and sex, with the ages of the subjects ranging from 15 to 60 years old and six females and ten males included in the study. Table 6 provides the category of classification, the number of samples, the labels, and the locations for which the data was collected. Table 6 is based on a 900 second optimal window size, which will be addressed in the data pre-processing section of this work.

Data Pre-Processing

The entire CM-PIR system is presented as a flowchart with Figure 13. The data pre-processing process is highlighted in this figure, where the green blocks relate to both human presence detection and biometric authentication classifications, and the orange corresponds to only the biometric authentication classification. Following the data collection of sixteen subjects in nine different ambient environments, various processes needed to be completed towards a stationary human presence detection and biometric authentication system based on the chest movement of the human subjects.

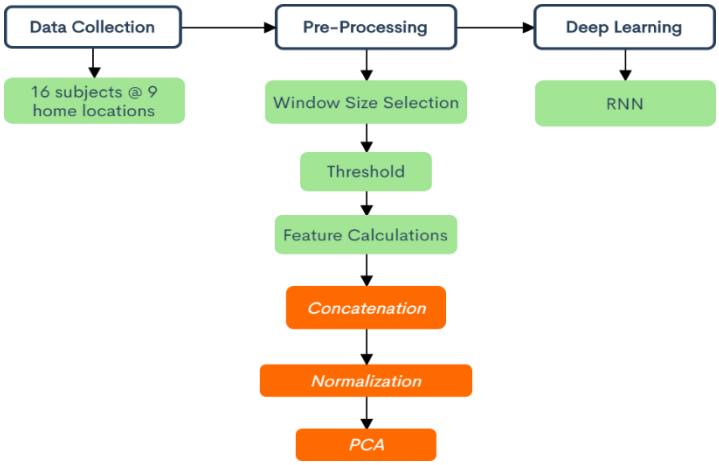

Figure 13. Flowchart for the CM-PIR system, including the many steps in the pre-processing stage. The green flowchart blocks represent both classifications, whereas orange relates to biometric authentication only.

To start, an optimal window size selection was needed for increased classification accuracy. The optimal window size was determined experimentally, by feeding various sizes to

the RNN deep learning model. A smaller window size selection increases the number of data samples available for training, for which deep learning models are dependent on, but the decrease in window size also limits the number of data points available for learning. This balance needs to be addressed, and experimentally, the optimal window size was found to be 90 seconds, which corresponds to 900 data points based on the 10 Hz sampling rate.

Early data collection of perfectly motionless human subjects shows waveforms that exist between 3.5 V and 1.5 V. Thus, to ensure that the waveforms learned from for both classifications is based on the chest movement only, a 3.5 V to 1.5 V threshold is applied to the raw PIR voltage data. This threshold was determined by early data collection results, as perfectly motionless human subjects resulted in voltages ranging from 3.0 to 2.0 V. To handle various ambient environments, with potentially greater ambient signal power, the threshold was determined to be optimal in the 3.5 to 1.5 V range. This threshold is added to the Python code, for which any 900 second data batch that includes values greater or less than this defined threshold is deleted. After the threshold is applied to the dataset, the number of data samples available for the 70% training, 15% testing, and 15% validation split is reduced from 566 to 417. This threshold completely removes four human subjects and three ambient environments from the dataset due to errors in data collection, including the constant movement of the volunteer during data collection. Figure 14 visually represents the purpose of applying the threshold to the data, for which there previously exists a non-chest movement waveform for the adversarial user labeled as “2” in Figure 14 (a) and only chest movement data in Figure 14 (b). The adversarial blue waveform in Figure 14 (a) is removed from the dataset with the applied threshold. Figure 14 is presented with a reduced window size for visualization purposes only.

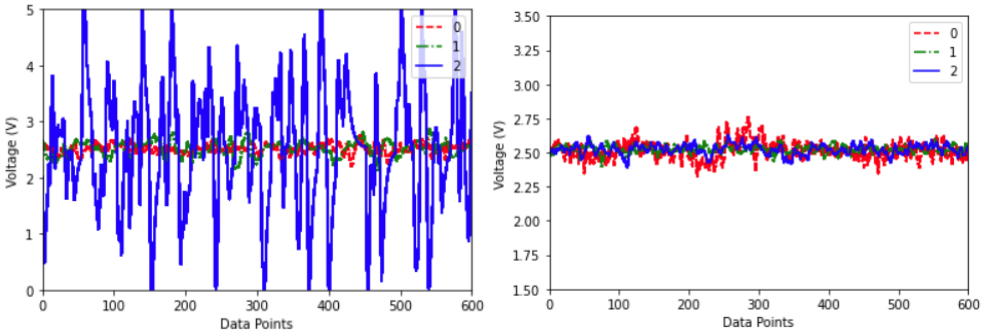

Figure 14. The raw PIR voltage data (a) before the applied threshold and (b) after the applied threshold.

Following the optimal window size selection and the applied threshold, the next step in the data pre-processing stage for the CM-PIR system is the feature engineering process towards greater classification accuracy. As presented in Figure 14 (b), there represents no obvious visual differences between the unoccupied scenario ("0") and the occupied scenarios ("1" and "2") via the raw voltage data. Due to this, various features were calculated during the pre-processing stage to determine the optimal combination for the greatest classification accuracy. Due to the success of the signal power feature for the stationary human presence detection classification with the MI-PIR system, the same feature is calculated for the CM-PIR system and utilized for the same purpose. Figure 15 presents the scenario for all three labels that is utilized for biometric authentication with the signal power feature. From Figure 15, the unoccupied scenario shows the greatest signal power, which deviates from the results of the MI-PIR system. This result is due to the applied threshold for which all data has similar raw voltage magnitude and due to the multiple ambient environments included in the dataset. These three example waveforms could potentially be from different ambient environments, causing the unoccupied scenario to show the greatest signal power. Due to these deviations that are present in the dataset, two conclusions can be drawn. The first conclusion drawn from Figure 15 is that the RNN deep learning model will have to learn from the unique waveforms that exist between the six ambient environments that are included after

the applied threshold. The second conclusion is that there exists a need for further feature calculations to potentially enhance the accuracies of the classifications made with the CM-PIR system.

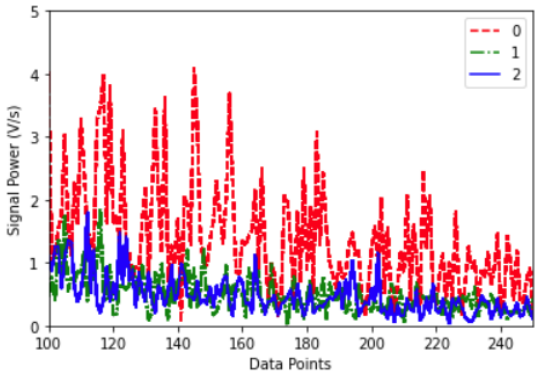

Figure 15. The signal power of the CM-PIR threshold data for each biometric authentication label.

Two additional features were calculated for and utilized for the biometric authentication classification only. These specific features include the novel acceleration filter presented in (3) and the discrete wavelet transform (DWT). As traditional biometric authentication systems are dependent on heart-related features, the extraction of the heart-rate signal via the novel acceleration filter is appended to the array of signal power values. Further, due to the DWT showing promise as a feature in related systems, this value is also appended to the feature array. In all, the feature array for biometric authentication includes 2,700 values following the appending of three features of 900 data points.

As shown in Figure 13 with the CM-PIR flowchart, there are two additional steps needed to complete the biometric authentication pre-processing stage. Utilizing the sklearn min max normalization again to map the raw signal power values from zero to one, the combined feature set including 2,700 data points is normalized before dimensionality reduction. This ensures that the magnitude of each calculated feature has equal importance for training. Finally, PCA is used for dimensionality reduction to specifically reduce the number of total samples from 2,700 data

points to five components. PCA is a simple linear autoencoder technique that serves to reduce the dimensionality of features and is often utilized for such purposes in deep learning applications. In all, the stationary human presence classification contains a feature set of 900 raw signal power values and the biometric authentication classification contains a feature set of five PCA components from a normalized 2,700 feature set consisting of the raw signal power, heart-rate magnitude, and the DWT. Both feature sets will be applied to the RNN deep learning model for their respective classifications.

Deep Learning

Due to the success of the RNN deep learning model with the MI-PIR sensor data, a similar model is developed for the CM-PIR system. The RNN deep learning model developed for the CM-PIR system is similar in architecture to the RNN model presented in Figure 6 (b). The RNN model is utilized to learn from the complex scenarios involved in a chest motion human monitoring system and is composed of two LSTM layers, three dropout layers, and two dense layers, exact to that of the RNN model presented in Figure 6 (b). The only difference between this RNN architecture is that the dropout layers have weights of 0.1 and not the 0.2 utilized for the MI-PIR activity recognition classification. The dropout layers were necessary in the classification of biometric authentication due to the potential overfitting with the limited data. In all, both classifications underwent 125 epochs for training and the results of the classifications are presented below.

Human Presence

The stationary human presence classification using the raw signal power of the chest movement of the various human subjects included in the dataset proved 94% accurate. The classification report for the human presence classification with the CM-PIR system is presented

below in Table 7. From Table 7, there are 63 samples utilized for testing, with 19 being an unoccupied scenario and 44 being an occupied scenario. This classification report presents not only the accuracy of the classification, but also the precision, recall, F1 score, and support for each label.

Table 7. Classification report for the CM-PIR stationary human presence detection classification.

	Precision	Recall	F1 Score	Support
0	0.86	0.95	0.90	19
1	0.98	0.93	0.95	44
Accuracy			0.94	63
Macro Avg.	0.92	0.94	0.93	63
Weighted Avg.	0.94	0.94	0.94	63

With no additional hardware needed, the CM-PIR is an even easier implementation of solving the stationary human presence classification using only one PIR sensor. Relying on the chest movement at a proposed desk situation in an at-home environment or at a desk location in an office environment proves that the CM-PIR system could learn from more complex movements that are of greater magnitude than the chest movement that is clamped between 3.5 V and 1.5 V. Based on these results, CM-PIR proves to be an accurate system for stationary human presence detection.

Biometric Authentication

The biometric authentication classification of classifying a verified user against an unoccupied scenario and all other adversarial users proves to be 75% accurate. The classification report for this classification is presented below in Table 8. Table 8 also presents the accuracy, precision, recall, F1 score, and support for each label in the dataset. The data for this classification is heavily balanced, with 15 data samples of the unoccupied scenario (“0”), 20 samples of the

verified user (“1”), and 28 samples of the adversarial users (“2”) utilized for a combined 63 samples for testing.

Table 8. Classification report for the CM-PIR biometric authentication classification.

	Precision	Recall	F1 Score	Support
0	0.76	0.87	0.81	15
1	0.71	0.75	0.73	20
2	0.76	0.68	0.72	28
Accuracy			0.75	63
Macro Avg.	0.75	0.77	0.75	63
Weighted Avg.	0.75	0.75	0.74	63

There are various solutions that could be implemented to potentially increase the initial accuracy of the biometric authentication classification with the CM-PIR system. For starters, collecting the chest movements of various subjects in various ambient environment causes many more scenarios to learn from, especially considering that the PIR sensor data is heavily dependent on the ambient environment. However, collecting these various environments allows for the CM-PIR system to be much more robust to various environments than other authentication systems. Also, a data verification step is proposed to increase the accuracy of the CM-PIR biometric authentication classification. With four human subjects being removed from the applied threshold completely, this indicates potential errors in the data or in the data collection as the human subjects should be remaining more motionless during the data acquisition stage. Lastly, more detailed feature engineering and data pre-processing will be addressed with potentials in raw voltage data normalization and spectrogram feature calculations.

System Quantifications

For more accurate comparisons with the MI-PIR system and other PIR systems in literature, the maximum sensing distance is quantified for the CM-PIR system. Subject A from Table 6 collects data at Location D and sits at iterative distances away (1 m, 2 m, and 3 m) from

the CM-PIR system with equal number of unoccupied samples for a balanced training set. Each location includes 30 minutes of continuous recording of Subject A, who remains completely motionless throughout the data acquisition. The results of this quantification show 1 m to be the maximum sensing distance for at 3 m the accuracy was 85% and at 2 m the accuracy was 92%. The 1 m sensing distance for this quantification proved 96% accurate, indicating the slight increase in accuracy with only one ambient environment included in the study. From these results, the 1 m distance is verified to be the optimal distance, as well as the maximum sensing distance.

Visualizations

Towards a greater understanding of the accuracy obtained with the CM-PIR system, as well as for potential work for increasing the biometric authentication classification accuracy, visualizations of the CM-PIR data are presented in this section. Previously, the raw signal power was presented in Figure 15, indicating that the unique waveforms are required for classification, as the unoccupied scenario showed greater signal power than that of the human subject present. Towards greater explainability, the Explainx library is utilized in Python to produce an understanding of the input features on the biometric authentication accuracy. Figure 16 presents the results of the Explainable AI method for the CM-PIR system on biometric authentication accuracy, where the “Raw” label corresponds to raw PIR voltage and “WWW” corresponds to the heart magnitude extracted with the novel acceleration filter. Towards the production of Figure 16, the sum of each input array is inputted for an importance quantification. From Figure 16, one can determine that the FFT signal power feature proves to be the strongest indicator of human presence, which aligns with the results from the MI-PIR system.

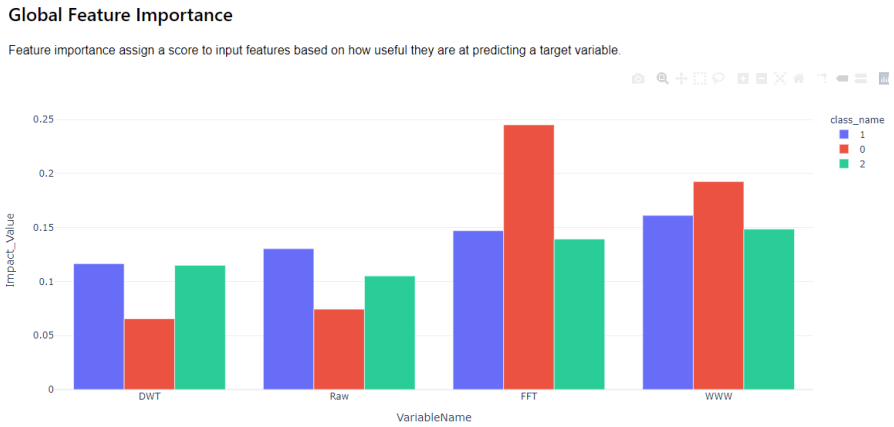

Figure 16. Global feature importance extracted from the Explainx library in Python, showing the FFT feature to be a strong indicator of human presence.

In understanding the importance of the ambient environment on the biometric authentication classification, a PCA visualization and confusion matrix comparison is presented. For the comparison, two datasets are compared: the entire dataset previously introduced and a dataset composed of only Location D. For the latter dataset, the optimal window size was selected to be ten seconds, as the number of samples at 90 seconds is limited at one location. Figure 17 presents the results of the PCA visualization for Figure 17 (a) of only one ambient environment and Figure 17 (b) of six different ambient environments. From this visualization, there is an evident increase in clustering ability with only one ambient environment to learn from.

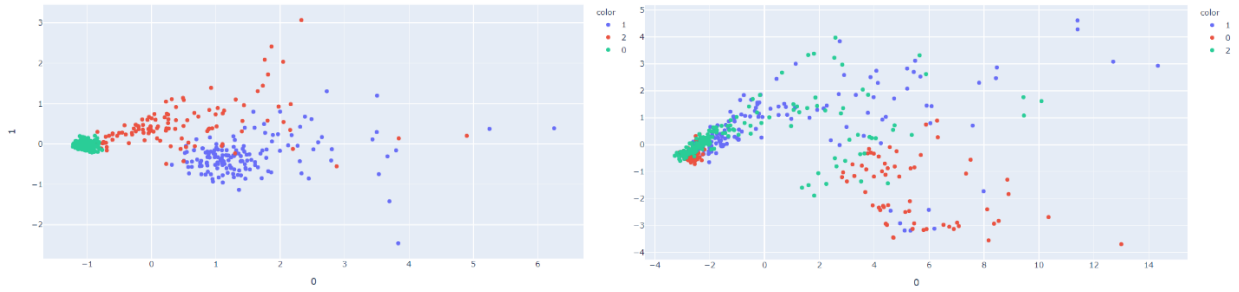

(a) (b)

Figure 17. PCA visualizations for (a) one ambient environment and (b) six ambient environments.

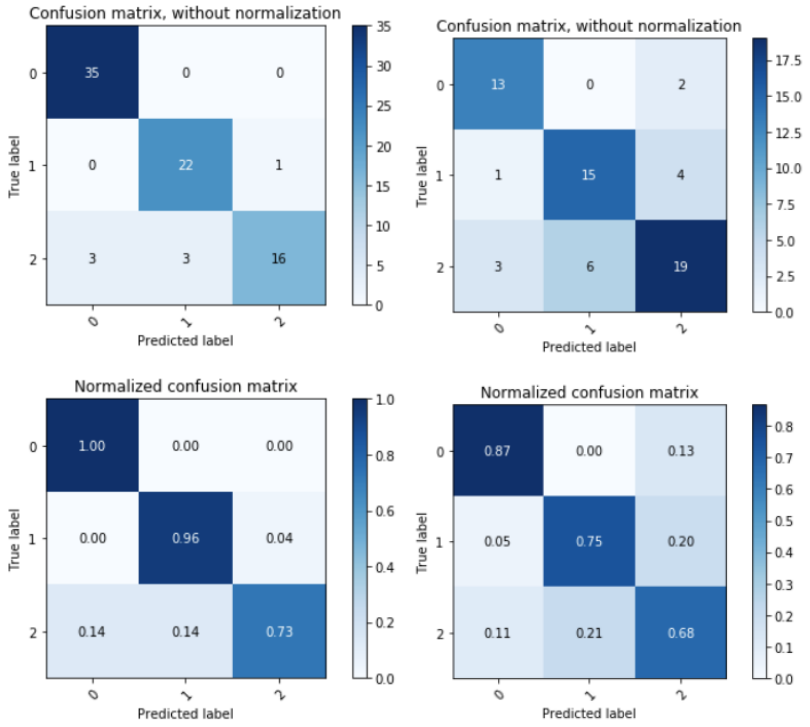

Figure 18. Biometric authentication confusion matrix for (a) only ambient environment and (b) six different ambient environments.

The confusion matrices from the outputs of the input features in both scenarios are presented in Figure 18, where Figure 18 (a) presents the confusion matrix of only one ambient environment with ten second data samples and Figure 18 (b) presents the confusion matrix for six different ambient environments with ninety second data samples. The accuracy from only one ambient environment was found to be 91% and the accuracy from the six different ambient environments with multiple human subjects was found to be 75%, as indicated previously. Although there is a significant increase with less ambient environments and human subjects, an authentication system is required to learn from the deviations presented in ambient environments and with additional possible adversaries. Proposed solutions to handle the various ambient environments include the normalization of raw PIR voltage data or the addition of an environment

discriminator to the loss function of the RNN deep learning model, as shown to be a successful approach in [27].

For a greater classification accuracy with the multiple ambient environments, various features have been experimented with. One feature that has shown some initial promise as a biometric authentication feature for greater classification accuracy is the high-resolution spectrogram. This feature is utilized in [45] for COVID-19 non-contact respiration monitoring, which provides promise in our work as a non-contact method of differentiating human subjects. Figure 19 presents the early representations of the spectrogram for an unoccupied, verified user, and a potential adversary at Location D. The unique visualizations of each label provide some level of promise for this feature for greater biometric authentication classification accuracy, and this feature will be experimented with further towards handling multiple ambient environments in the biometric authentication classification.

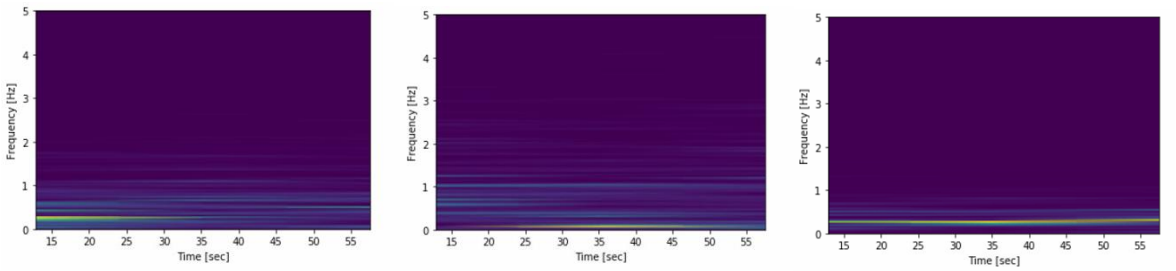

(a) (b) (c)

Figure 19. Spectrogram for (a) unoccupied, (b) verified user, and (c) adversary at Location D.

Discussion

Presented in this thesis is two novel systems to combat the stationary human presence detection issue surrounding the use of a single PIR sensor for monitoring applications. Both MI-PIR and CM-PIR proved accurate at stationary human presence detection using a single PIR sensor, proving 100% and 94% accurate, respectively. For the MI-PIR system, the maximum

sensing distance is found experimentally to be 21 m and the horizontal FoV is increased due to the rotating nature of the system from 93 degrees to an overall 223 degrees of detection. These expansions in maximum sensing distance and horizontal FoV are much greater than related works in [17], [19], without the need for a complex mechanical structure. CM-PIR even requires no additional hardware in its implementation. The complete comparison of the various solutions for stationary human presence detection with a single PIR sensor can be compared in Table 9.

Table 9. Comparisons of the proposed solutions for stationary human presence detection using a single PIR sensor.

Classification	Reference	Proposed Solution	Methods	Horizontal FoV (˚)	Max. Sensing (m)	Accuracy (%)
Stationary Human Presence	[17]	Optical Shutter	Presence – Voltage	110	7	100
	[19]	Optical Shutter	Presence – Voltage	93	4.5	100
	MI-PIR	Motion-Induced	Classification – RNN	223	21	100
	CM-PIR	Chest Motion	Presence - RNN	93	1	94

In comparison of PIR systems for activity recognition using limited PIR sensors only, Table 10 summarizes these systems. The system proposed in [19] utilizes an optical shutter PIR sensor to categorize three activities of unoccupied, sitting, and walking with 93% accuracy. The system in [19] shows superiority to the MI-PIR system as it recognizes activities in a continuous data collection with multiple subjects; however, the efficacy of the MI-PIR system at recognizing multiple activities in a residential environment proves superior in an at-home monitoring activity recognition solution. In terms of a residential environment, the *ALPAS* system in [22] reports a F-measure of 57% for recognizing multiple activities performed on a sofa. The MI-PIR solution, in comparison, recognizes six different activities with a 98% accuracy in a residential environment. Although the system in [22] recognizes multiple activities at one location, the much inferior performance shows that the MI-PIR system is a much more effective approach to activity recognition using a single PIR sensor.

Table 10. Comparison of activity recognition systems using PIR sensors.

Classification	Reference	# of PIRs	# of Activities	Activities	Results
HAR - Office	[19]	1	3	-Unoccupied -Sitting -Walking	93% Accuracy
	MI-PIR	1	3	-Unoccupied -Sitting -Walking	100% Accuracy
HAR – Residential	[22]	2	4	-Eat on Sofa -Read of Sofa -Use Phone on Sofa -Use PC on Sofa	57% F-Measure
	MI-PIR	1	6	-Unoccupied -Working at Desk -Laying on Ground -Exercise on Ground -Watch TV on Bed -Sleep on Bed	98% Accuracy

The biometric authentication classification results for the CM-PIR system and related solutions proposed in literature is compared with Table 11. First, the proposed solution in [37] utilizes facial features extracted from a video capturing modality to achieve a mean authentication performance of 86.67% based on PPG-based features from multiple environments. The proposed solution based on a respiration-related feature achieves 100% accuracy using a SVM machine learning model, an active Doppler radar, and one ambient environment. Likewise, the proposed solution in [39] utilizes an active Doppler radar and one ambient environment to achieve a biometric authentication classification accuracy of 98.61% accuracy based on a heart-related feature. In comparison to these solutions in literature, the CM-PIR system authenticates twelve subjects in six different home locations, proving to be a robust solution to authentication, based on the addition of five different home environments. As with the work in [37], the video capturing in multiple environments is more robust, but is privacy intrusive. Furthermore, the CM-PIR system is the only system based on a passive sensor modality, where the other proposed sensor modalities

raise health and energy related concerns. Increasing the accuracy of the CM-PIR system will make the proposed solution more effective for an IoT security solution.

Table 11. Comparison of non-contact biometric authentication systems.

Reference	Proposed Solution	Feature	Subjects	Locations	Accuracy (%)
[37]	Video	PPG	20	Multiple	86.67
[38]	Doppler radar	Respiration	12	1	100
[39]	Doppler radar	Heart	78	1	98.61
CM-PIR	PIR	Chest/Heart	12	6	75

Conclusions

Elderly monitoring remains a growing challenge due to both the growing prevalence of neurodegenerative diseases in these populations and the growing age of the world population. To monitor elderly individuals effectively and continuously in an at-home environment, there exist a need for a solution that is cheap, accurate, passive, non-contact, and non-intrusive. Ambient sensor modalities with statistical learning algorithms have been proposed in literature to meet these specified needs, yet many of these solutions are still inaccurate, expensive, or utilize active sensor modalities. The proposed MI-PIR sensor solution, which requires one PIR sensor and a robotic actuator, fills the gaps in literature and shows early promise as an elderly monitoring solution in this work. Monitoring systems need to accurately monitor elderly individuals for a greater state of mind for both caregivers and the hospital systems. The MI-PIR system has shown highly accurate classification results with an RNN deep learning model for activity recognition in two different ambient environments, with specialization for an elderly monitoring situation through the classification of a potential fall scenario. For indoor localization, a GPR model showed effective visual clustering in both ambient environments. In this case, MI-PIR can be effective for an at-home elderly monitoring solution.

As the number of connected devices increase, the security of these devices remains a challenge. For at-home continuous monitoring solutions, there exists a need for a cheap, passive, non-intrusive, and accurate security system. Where fingerprints can be easily replicated and facial recognition systems are intrusive, a biometric authentication system that utilizes a passive sensor modality is seen as a more advantageous approach. Towards this end, the CM-PIR system achieves 75% accuracy between six different ambient environments. Utilizing a heart-related biometric feature, the CM-PIR system is also a detection of liveliness, showing effective at comparing unoccupied and occupied scenarios.

Both MI-PIR and CM-PIR expand the functionalities of PIR sensors as they have shown effective at stationary human presence detection. MI-PIR can detect stationary human occupants with 100% classification accuracy at 36 second scan times. CM-PIR can detect stationary human occupants from six different ambient environments at a 94% classification accuracy, requiring no additional hardware. MI-PIR additionally expands the maximum sensing distance and horizontal FoV of conventional PIR sensor systems.

This thesis introduces two novel systems for stationary human presence detection and related human monitoring applications. The proposed MI-PIR system is successful at room occupancy classification, occupancy count estimation, distinct location classification, human target differentiation, activity recognition, and precise indoor localization with the utilization of statistical learning algorithms for differentiation of the multiple scenarios that exists between various ambient conditions. Further, the CM-PIR system proves accurate at stationary human presence and biometric authentication via a RNN deep learning model with LSTM units. These results prove these systems are effective solutions for the stationary human presence detection with a single PIR sensor, as well as various human monitoring applications.

Acknowledgements

This research is supported by AFOSR grant FA9550-18-1-0287.

References

[1] E. Burns and R. Kakara, "Deaths from Falls Among Persons Aged ≥65 Years — United States, 2007–2016," *MMWR. Morbidity and Mortality Weekly Report*, vol. 67, no. 18, May 2018, doi: 10.15585/mmwr.mm6718a1.

[2] D. of E. and S. A. P. D. United Nations, "World Population Ageing 2019," *(ST/ESA/SER.A/444)*, 2020, Accessed: Dec. 30, 2020. [Online]. Available: https://www.un.org/development/desa/pd/sites/www.un.org.development.desa.pd/files/files/documents/2020/Jan/un_2019_worldpopulationageing_report.pdf.

[3] M. de Nardi, E. French, J. B. Jones, and J. McCauley, "Medical Spending of the Elderly," *National Bureau of Economic Research*, Jun. 2015. https://www.nber.org/bah/2015no2/medical-spending-elderly#:~:text=Medical%20spending%20by%20the%20elderly,percent%20of%20all%20medical%20spending (accessed Dec. 30, 2020).

[4] M. S. Obaidat, S. P. Rana, T. Maitra, D. Giri, and S. Dutta, "Biometric Security and Internet of Things (IoT)," in *Biometric-Based Physical and Cybersecurity Systems*, Obaidat Mohammad S., I. Traore, and I. Woungang, Eds. Cham: Springer International Publishing, 2019, pp. 477–509.

[5] M. N. Alraja, M. M. J. Farooque, and B. Khashab, "The Effect of Security, Privacy, Familiarity, and Trust on Users' Attitudes Toward the Use of the IoT-Based Healthcare: The Mediation Role of Risk Perception," *IEEE Access*, vol. 7, 2019, doi: 10.1109/ACCESS.2019.2904006.

[6] J. Andrews, M. Kowsika, A. Vakil, and J. Li, "A Motion Induced Passive Infrared (PIR) Sensor for Stationary Human Occupancy Detection," in *2020 IEEE/ION Position, Location and Navigation Symposium (PLANS)*, Apr. 2020, pp. 1295–1304.

[7] J. Andrews, A. Vakil, and J. Li, "Biometric Authentication and Stationary Detection of Human Subjects by Deep Learning of Passive Infrared (PIR) Sensor Data," Dec. 2020.

[8] E. Topol, *Deep Medicine*. Basic Books, 2019.

[9] X. Liu, T. Yang, S. Tang, P. Guo, and J. Niu, "From relative azimuth to absolute location," Apr. 2020, doi: 10.1145/3372224.3380878.

[10] B. Mukhopadhyay, S. Srirangarajan, and S. Kar, "Modeling the analog response of passive infrared sensor," *Sensors and Actuators A: Physical*, vol. 279, Aug. 2018, doi: 10.1016/j.sna.2018.05.002.

[11] R. K. Hobbie and B. J. Roth, *Intermediate physics for medicine and biology, fifth edition*. Springer International Publishing, 2015.

[12] J. W. Clark *et al.*, *Medical Instrumentation: Application and Design*, 4th ed. Wiley, 2009.

[13] X. Xu, Y. Liang, P. He, and J. Yang, "Adaptive Motion Artifact Reduction Based on Empirical Wavelet Transform and Wavelet Thresholding for the Non-Contact ECG Monitoring Systems," *Sensors*, vol. 19, no. 13, Jul. 2019, doi: 10.3390/s19132916.

[14] A. Vakil, "Heterogenous Multimodal Sensor Fusion via Canonical Correlation Analysis and Explainable AI," Rochester, 2020.

[15] A. Adadi and M. Berrada, "Peeking Inside the Black-Box: A Survey on Explainable Artificial Intelligence (XAI)," *IEEE Access*, vol. 6, 2018, doi: 10.1109/ACCESS.2018.2870052.

[16] X. Hong, J. Gao, X. Jiang, and C. J. Harris, "Estimation of Gaussian process regression model using probability distance measures," *Systems Science & Control Engineering*, vol. 2, no. 1, Dec. 2014, doi: 10.1080/21642583.2014.970731.

[17] R. O. S. Juan, J. S. Kim, Y. H. Sa, H. S. Kim, and H. W. Cha, "Development of a Sensing Module for Standing and Moving Human Body Using a Shutter and PIR Sensor," *International Journal of Multimedia and Ubiquitous Engineering*, vol. 11, no. 7, Jul. 2016, doi: 10.14257/ijmue.2016.11.7.05.

[18] L. Wu, F. Gou, S.-T. Wu, and Y. Wang, "SLEEPIR: Synchronized Low-Energy Electronically Chopped PIR Sensor for True Presence Detection," *IEEE Sensors Letters*, vol. 4, no. 3, Mar. 2020, doi: 10.1109/LSENS.2020.2976801.

[19] L. Wu and Y. Wang, "A Low-Power Electric-Mechanical Driving Approach for True Occupancy Detection Using a Shuttered Passive Infrared Sensor," *IEEE Sensors Journal*, vol. 19, no. 1, Jan. 2019, doi: 10.1109/JSEN.2018.2875659.

[20] M. Pham, D. Yang, and W. Sheng, "A Sensor Fusion Approach to Indoor Human Localization Based on Environmental and Wearable Sensors," *IEEE Transactions on Automation Science and Engineering*, vol. 16, no. 1, Jan. 2019, doi: 10.1109/TASE.2018.2874487.

[21] M. Gochoo, T.-H. Tan, V. Velusamy, S.-H. Liu, D. Bayanduuren, and S.-C. Huang, "Device-Free Non-Privacy Invasive Classification of Elderly Travel Patterns in A Smart House Using PIR Sensors and DCNN," *IEEE Sensors Journal*, 2017, doi: 10.1109/JSEN.2017.2771287.

[22] Y. Kashimoto, M. Fujiwara, M. Fujimoto, H. Suwa, Y. Arakawa, and K. Yasumoto, "ALPAS: Analog-PIR-Sensor-Based Activity Recognition System in Smarthome," Mar. 2017, doi: 10.1109/AINA.2017.33.

[23] D. Li, J. Liu, S. Nishimura, Y. Hayashi, J. Suzuki, and Y. Gong, "Multi-Person Action Recognition in Microwave Sensors," Oct. 2020, doi: 10.1145/3394171.3413801.

[24] S. Singh and B. Aksanli, "Non-Intrusive Presence Detection and Position Tracking for Multiple People Using Low-Resolution Thermal Sensors," *Journal of Sensor and Actuator Networks*, vol. 8, no. 3, Jul. 2019, doi: 10.3390/jsan8030040.

[25] S. Kim, S. Kang, K. R. Ryu, and G. Song, "Real-time occupancy prediction in a large exhibition hall using deep learning approach," *Energy and Buildings*, vol. 199, Sep. 2019, doi: 10.1016/j.enbuild.2019.06.043.

[26] T. Li, L. Fan, M. Zhao, Y. Liu, and D. Katabi, "Making the Invisible Visible: Action Recognition Through Walls and Occlusions," Oct. 2019, doi: 10.1109/ICCV.2019.00096.

[27] L. Fan, T. Li, R. Fang, R. Hristov, Y. Yuan, and D. Katabi, "Learning Longterm Representations for Person Re-Identification Using Radio Signals," Jun. 2020, doi: 10.1109/CVPR42600.2020.01071.

[28] L. Fan, T. Li, Y. Yuan, and D. Katabi, "In-Home Daily-Life Captioning Using Radio Signals," Aug. 2020.

[29] J. Liu *et al.*, "Human Occupancy Detection via Passive Cognitive Radio," *Sensors*, vol. 20, no. 15, Jul. 2020, doi: 10.3390/s20154248.

[30] H. Zou, Y. Zhou, J. Yang, and C. J. Spanos, "Towards occupant activity driven smart buildings via WiFi-enabled IoT devices and deep learning," *Energy and Buildings*, vol. 177, Oct. 2018, doi: 10.1016/j.enbuild.2018.08.010.

[31] X. Wang, X. Wang, S. Mao, J. Zhang, S. C. G. Periaswamy, and J. Patton, "Indoor Radio Map Construction and Localization With Deep Gaussian Processes," *IEEE Internet of Things Journal*, vol. 7, no. 11, Nov. 2020, doi: 10.1109/JIOT.2020.2996564.

[32] G. Zhang, P. Wang, H. Chen, and L. Zhang, "Wireless Indoor Localization Using Convolutional Neural Network and Gaussian Process Regression," *Sensors*, vol. 19, no. 11, May 2019, doi: 10.3390/s19112508.

[33] X. He, D. Aloi, and J. Li, "Portable 3D visual sensor based indoor localization on mobile device," Jan. 2016, doi: 10.1109/CCNC.2016.7444947.

[34] Q. Zhang, "Deep Learning of Electrocardiography Dynamics for Biometric Human Identification in era of IoT," Nov. 2018, doi: 10.1109/UEMCON.2018.8796676.

[35] D. Wang, Y. Si, W. Yang, G. Zhang, and T. Liu, "A Novel Heart Rate Robust Method for Short-Term Electrocardiogram Biometric Identification," *Applied Sciences*, vol. 9, no. 1, Jan. 2019, doi: 10.3390/app9010201.

[36] Y. Li, Y. Pang, K. Wang, and X. Li, "Toward improving ECG biometric identification using cascaded convolutional neural networks," *Neurocomputing*, vol. 391, May 2020, doi: 10.1016/j.neucom.2020.01.019.

[37] O. R. Patil, W. Wang, Y. Gao, W. Xu, and Z. Jin, "A Non-Contact PPG Biometric System Based on Deep Neural Network," Oct. 2018, doi: 10.1109/BTAS.2018.8698552.

[38] S. M. M. Islam, A. Rahman, N. Prasad, O. Boric-Lubecke, and V. M. Lubecke, "Identity Authentication System using a Support Vector Machine (SVM) on Radar Respiration Measurements," Jun. 2019, doi: 10.1109/ARFTG.2019.8739240.

[39] F. Lin, C. Song, Y. Zhuang, W. Xu, C. Li, and K. Ren, "Cardiac Scan," Oct. 2017, doi: 10.1145/3117811.3117839.

[40] S. M. M. Islam, O. Borić-Lubecke, Y. Zheng, and V. M. Lubecke, "Radar-Based Non-Contact Continuous Identity Authentication," *Remote Sensing*, vol. 12, no. 14, Jul. 2020, doi: 10.3390/rs12142279.

[41] H. Kapu, K. Saraswat, Y. Ozturk, and A. E. Cetin, "Resting heart rate estimation using PIR sensors," *Infrared Physics & Technology*, vol. 85, Sep. 2017, doi: 10.1016/j.infrared.2017.05.010.

[42] Z. Huang, Y. Liu, Y. Fang, and B. K. P. Horn, "Video-based Fall Detection for Seniors with Human Pose Estimation," Oct. 2018, doi: 10.1109/UV.2018.8642130.

[43] Z. Kabelac *et al.*, "Passive Monitoring at Home: A Pilot Study in Parkinson Disease," *Digital Biomarkers*, vol. 3, no. 1, Apr. 2019, doi: 10.1159/000498922.

[44] C. K. Alexander and M. N. O. Sadiku, *Fundamentals of electric circuits*. .

[45] F. Li, M. Valero, H. Shahriar, R. A. Khan, and S. I. Ahamed, "Wi-COVID: A COVID-19 symptom detection and patient monitoring framework using WiFi," *Smart Health*, vol. 19, Mar. 2021, doi: 10.1016/j.smhl.2020.100147.